DISCLAIMER NOTICE

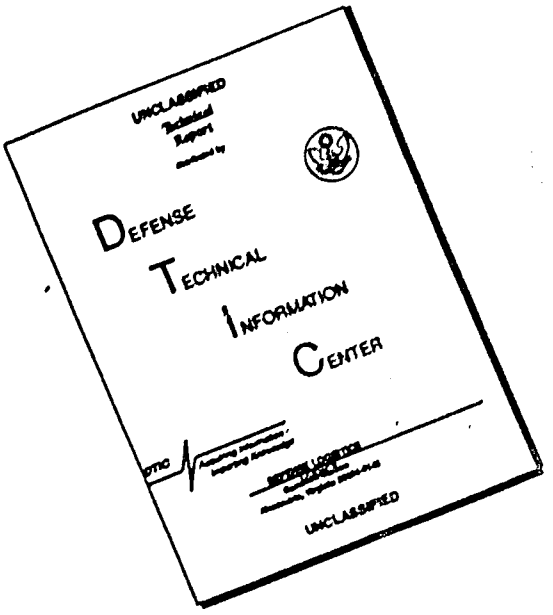

THIS DOCUMENT IS BEST QUALITY AVAILABLE. THE COPY FURNISHED TO DTIC CONTAINED A SIGNIFICANT NUMBER OF PAGES WHICH DO NOT REPRODUCE LEGIBLY.

64-12

RADC-TDR-64-58

MULTIMEGAWATT BROADBAND MICROWAVE TUBES

TECHNICAL DOCUMENTARY REPORT NO. RADC-TDR-64-58
March 1964

Techniques Branch
Rome Air Development Center
Research and Technology Division
Air Force Systems Command
Griffiss Air Force Base, New York

Project No. 5573, Task No. 557303

(Prepared under Contract No. AF30(602)-2575 by Stanford University, Microwave Laboratory, W.W. Hansen Laboratories of Physics)

DDC AVAILABILITY NOTICE

Qualified requesters may obtain copies from the Defense Documentation Center (TISIR), Cameron Station, Alexandria, Va., 22314. Orders will be expedited if placed through the librarian or other person designated to request documents from DDC.

Releasable to OTS.

LEGAL NOTICE

When US Government drawings, specifications, or other data are used for any purpose other than a definitely related government procurement operation, the government thereby incurs no responsibility nor any obligation whatsoever; and the fact that the government may have formulated, furnished, or in any way supplied the said drawings, specifications, or other data is not to be regarded by implication or otherwise, as in any manner licensing the holder or any other person or corporation, or conveying any rights or permission to manufacture, use, or sell any patented invention that may in any way be related thereto.

DISPOSITION NOTICE

Do not return this copy. Retain or destroy.

FOREWORD

This report describes the results achieved under Contract AF 30(602)-2575 during the second contract year, November 1, 1962 to October 31, 1963.

One of the specific overall objectives of this contract is to conduct theoretical and experimental investigations of microwave tubes with a view toward the development of tubes capable of at least 10 megawatts of peak power, average power approaching 50 kilowatts, bandwidths approaching 30 per cent, gains of 35 db, and efficiencies of 40 per cent. A more general objective is to investigate new methods of achieving either high peak and average power, large bandwidths, or high frequencies by either new methods or by unconventional extensions of existing approaches.

During the course of this contract year, three quarterly memoranda were written and distributed:

(1) Quarterly Status Report No. 5, for the period 1 November 1962 to 31 January 1963 (Microwave Laboratory Report No. 1012).

(2) Quarterly Status Report No. 6, for the period 1 February to 30 April 1963 (Microwave Laboratory Report No. 1037). This status report was also issued by RADC as Technical Documentary Report No. RADC-TDR-63-286.

(3) Quarterly Status Report No. 7, for the period 1 May to 31 July 1963 (Microwave Laboratory Report No. 1080).

This Annual Report summarizes the materials reported in these three quarterly status reports and describes the work done in the final quarterly period as well.

At the time of this Annual Report there were 8 projects active under this contract:

I. Oscillation Suppression in TWT's	V. Extended-interaction Klystrons
II. Centipede TWT	VI. Hollow Beam Guns
III. Long-slot TWT	VII. Transverse-wave Studies
IV. Nonperiodic Dielectric-lined TWT	VIII. Electron Beam Interaction with a Cesium Plasma

The Responsible Investigator for this contract is Professor Marvin Chodorow. The number for this report is M.L. No. 1116.

Suggested keyword list: Electronic Tube Devices, Traveling Wave Tubes, Klystrons

ABSTRACT

This report covers progress on the eight tasks which have been pursued during the second contract year. This includes (1) oscillation suppression in high power TWT's, (2) study of the centipede TWT structure, (3) improvement of stability of the long-slot TWT, (4) development of a non-periodic dielectric-line TWT, (5) development of extended-interaction klystrons, (6) study of hollow beam electron guns, (7) study of transverse-wave devices, and (8) investigation of electron beam interaction with a plasma.

In addition to the material presented in this report, each task will be discussed more fully in separate reports as "technical milestones" arise.

PUBLICATION REVIEW

This report has been reviewed and is approved. For further technical information on this project, contact EMATE, Extension 4251.

Approved: George H. Becker
GEORGE H. BECKER, 1/Lt, USAF
Project Engineer
Electron Devices Section

Approved: James W. Baldwin
for Lt Col USAF
ARTHUR J. FROHLICH
Chief, Techniques Branch
Surveillance & Control Division

ABSTRACTS

SECOND ANNUAL REPORT

I. OSCILLATION SUPPRESSION IN TWT'S

The electron stick has been used to evaluate methods of improving the stability characteristics of high-power TWT's. Of particular interest are the pulse-edge (π-point) oscillations. The technique applied to this problem is that of selectively coupling the periodic centipede structure to an external, lossless, uniform guide. The results of the theory and experiment are presented. A complete report of this project will be forthcoming as a technical report.

II. CENTIPEDE TWT

The centipede circuit has been adapted for use on the electron stick in such a manner that the amplitude and phase of the growing wave along the beam circuit interaction length can be measured. The results of this study will be of utmost value in optimizing the many parameters affecting the beam-circuit interaction. The circuit and associated equipment are ready for evaluation on the electron stick.

III. LONG-SLOT TWT

Several methods to improve the stability of the long-slot TWT have been studied and evaluated by cold-test measurements. Some of these have been evaluated on the electron stick. The results of these measurements are presented.

IV. NONPERIODIC DIELECTRIC-LINED TRAVELING-WAVE TUBES

An electron stick with a new, iron-plated tungsten helix has been completed and is being activated. The iron plating increases the rf

resistance of the wire tenfold. If, as predicted, the parasitic helix oscillations are suppressed, the new helix can, at last, serve as the rf-transparent beam-tunnel lining of nonperiodic extra-high-power S-band tubes based on rf structures that are simply uniform sleeves of dielectric inside a metal shell.

V. EXTENDED-INTERACTION KLYSTRONS

A three-cavity S-band hybrid tube, consisting of two tunable conventional klystron cavities, followed by an extended-interaction output resonator, was built and tested on the electron stick. With the output resonator adjusted for interaction over one resonant wavelength, the overall small-signal gain was found to be 19 db with a 3 db bandwidth of 3.5 %. Longer interaction lengths were made impractical both by parasitic oscillations on the electron stick and by the inherent difficulty of loading a long resonator sufficiently to prevent monotron instability. The two-cavity gain of the tunable bunching section remained at 11.0 ± 1.0 db over the frequency range of interest. Large-signal or saturation measurements were not made, due to arcing in the output resonator at the 30 kW level.

VI. HOLLOW BEAM GUNS

A promising method for the design of hollow beam guns is through the use of the paraxial ray equation. During the year this method was developed to second order with inclusion of magnetic fields, the only restriction on the magnetic field being that it must be tangential to the cathode. The superiority of this version of the paraxial ray method over previous work stems from the fact that the higher-order solutions of the space-charge flow are found by solving ordinary differential equations instead of partial differential equations.

VII. TRANSVERSE-WAVE STUDIES

The objective of this project is to study a possible approach to broadband high-power amplifiers, which involves interaction between an electron beam and a circuit in the presence of an axial dc magnetic field. The emphasis of this project has been shifted from ordinary transverse-wave

interaction towards investigation of the new force-free transverse waves which can propagate on rotating beams.

VIII. ELECTRON BEAM INTERACTION WITH A CESIUM PLASMA

The results of an experimental study of slow-wave propagation along a plasma column are discussed. This experimental study has been aimed at checking the propagation theory (summarized in the previous Annual Report) for a plasma column with a radial density variation. It was found possible to learn something about the plasma density profile from this study. An anomaly associated with attenuation of the slow waves propagating along a finite plasma column was investigated theoretically and experimentally. The anomaly appears to be well explained by the hypothesis of Landau damping in the plasma sheath as given by Pavkovich and Kino in their work on the rf theory of the plasma sheath. The theoretical study of the gain mechanism of the finite beam plasma interaction is summarized, and the design and purpose of some experimental beam-plasma tubes are discussed.

INTRODUCTION

The objectives of this contract can be broadly divided into two categories, one concerned with theoretical and experimental investigations of a particular class of microwave tubes designed for multimegawatt peak powers, and the second a more speculative group of projects which are intended to achieve high power, reasonable bandwidths, and possibly also very high frequencies by more unconventional means. Thus, of the eight projects described here, five of them deal with specific problems related to high power traveling-wave tubes or klystrons and are definitely concerned with improvement of operating characteristics which are not completely satisfactory in existing tubes. While the other three projects are concerned with the more basic investigations on the five specific projects, the following comments are relevant. The present state of development of high-powered broadband pulsed amplifiers is that, to a large extent, peak and average powers can be quite readily achieved and have been achieved both at Stanford and elsewhere. The principal deficiencies of the existing tubes are somewhat inadequate bandwidths and instabilities, that is, the presence of oscillations under certain operating conditions. A less serious but still important problem is that of efficiency, which, while quite satisfactory in existing tubes, is probably capable of improvement. Thus, the five specific projects are all aimed at these areas. Since these projects are not primarily concerned at the moment with high average power, it has been found possible to investigate many of the problems using a special device known as the "electron stick" which provides a separate vacuum for the electron beam and permits putting the interaction circuits external to the vacuum. This facilitates the investigation of various ideas concerned with oscillation suppression, of the saturation and efficiency characteristics of high power tubes, and of new circuits which may give better bandwidths. These five projects all use this "electron stick."

Project I is concerned with methods of investigating suppression of oscillation in a circuit which is a prototype of several successful high power traveling-wave tubes but which is still subject to oscillation under some conditions. Project II, using a particular TWT circuit, is concerned with the rate of growth of the current as a function of measuring distance in an output circuit in order to investigate the efficiency characteristics. Projects III and IV are concerned with circuits which may give considerably greater bandwidth and/or freedom from oscillation as compared with existing high power traveling-wave tube circuits. Project V investigates an amplifier, the extended interaction klystron, which uses unconventional cavities which are capable of giving greater bandwidths and also greater efficiency than conventional klystron cavities. Here also by use of the "stick" it is possible to investigate the effects of changes in circuit parameters on performance, using the same electron optics, which is a very important means of getting performance characteristics of this type of klystron. Project VI is concerned with hollow beam guns and continues earlier work on the design of unconventional beam optics by analytic methods leading to much higher perveance guns. Such guns would also achieve some of the objectives of this program, perturbing greater bandwidths with klystrons. Projects VII and VIII are concerned with unconventional devices which may lead to new types of high powered amplifiers. One uses transverse interaction of the electrons and the other is concerned with using interaction of an electron beam with a plasma as a means of achieving gain. Since both use electron interactions which are different than standard linear beam devices, the normal parameters which govern and limit the performance of normal linear beam devices would not apply. It is important to see what kinds of devices might be possible using these different types of interaction and to what extent these interactions would permit achieving characteristics beyond those of conventional traveling-wave tubes or klystrons.

TABLE OF CONTENTS

I. OSCILIATION SUPPRESSION IN TWT'S

A. INTRODUCTION

The objective of this study is to suppress the various types of oscillations that can occur in a periodic structure when it is excited by an electron beam (as in high-power traveling-wave tubes) without introducing excessive attenuation into the operating frequency band. Of particular interest are the pulse-edge (π-point) oscillations which are inherently possible in any TWT which utilizes certain types of periodic structures. The technique which is being applied to this problem is that of selectively coupling the periodic structure to an external, lossless, uniform waveguide. The selectivity is obtained by properly adjusting the phase and attenuation characteristics of the waveguide. The structure being studied in this case is the "centipede" structure, but this same technique could be applied to the particular oscillation problems of any other periodic structure such as the "cloverleaf" or the "long-slot."

B. DISCUSSION

The bulk of the experimental and theoretical work on this project has been completed and a comprehensive report which describes the important results that were obtained is being written. A small amount of experimental work remains to be done, and this is being carried on concurrently with the writing of the report. It is expected that this work will be concluded shortly, and hence the report should be ready for distribution in the near future. Since this report will describe the work in detail, only a summary of this work will be presented here.

1. Experimental Work

In the experimental portion of this study the "electron stick" was used to evaluate the effect of external loading on the oscillation gain

and bandwidth characteristics of the "centipede" structure. In particular, the effect of coupling an external, lossless waveguide to the structure by means of slots was studied. Also, a relative comparison between this scheme and two which were suggested by Ivanek[1] was also attempted. These other two schemes consisted of coupling by means of resonant slots to plain lossy material and to a lossy waveguide whose cutoff is near the π-point of the structure. The latter is similar to the method used for the long-slot structure (Part III of this report). A study of the oscillation and gain characteristics of the unloaded structure also had to be made in order to establish a basis of comparison, and this resulted in an increased understanding of the oscillatory behavior of the structure at a cutoff.

The oscillation characteristics of the unloaded structure were obtained by varying the length of the structure and observing the frequency and beam voltage at which the oscillations occurred. It was found that the oscillations first occurred at a frequency corresponding to the π-point (cutoff) of the structure. As the length was increased, the oscillations occurred over a wider band of frequencies and exhibited a typical backward-wave oscillation characteristic at frequencies away from the cutoff (no forward-wave oscillations were observed). This means that the structure is most unstable at frequencies near its cutoff points (this may be attributed to the resonant nature of the fields in the structure at these points). This explains why the pulse-edge oscillations which may occur when a high-power TWT is operated under pulsed conditions always have a frequency which corresponds to a structure cutoff. It is only at these points that the structure is unstable enough to allow oscillations to build up during the fast rise and fall times of the beam voltage pulse. Hence, to suppress these pulse-edge oscillations, it is only necessary to load the structure at the corresponding cutoff frequency.

The external, lossless waveguide which was used consisted of a standard X-band guide loaded by dielectric slabs ($\epsilon' = 15$) such that its dispersion characteristic passed through the π-point of the centipede structure. The slots in the structure were chosen to be the maximum length allowed by the

---

[1] F. Ivanek, Microwave Laboratory Report No. 1115, Stanford University (November 1963).

X-band size guide and were themselves loaded with dielectric ($\epsilon' \simeq 6$) so that the slots would produce a measurable effect on the start-oscillation length of the structure. Also, two sets of diametrically opposed slots (and hence two waveguides) were used.

A structure having 10 slotted sections showed about a 40% increase in start-oscillation length when coupled to the external, lossless waveguides. When coupled to the lossy waveguides and to the plain, lossy material, the start-oscillation length was increased by 10% and 20%, respectively. It is felt that the variations in starting length observed for the various schemes is due mainly to changes in the slot resonant frequency caused by changing the environment externally adjacent to the slots, rather than to fundamental differences in the methods of loading the structure. Further experiments will be carried out to determine the relative positions of the slot resonant frequencies which correspond to the various loading schemes.

The small-signal gain of the structure (with and without external loading schemes) was measured by observing the relative output of a small probe in the structure with the beam on and with the beam off. The probe was placed directly in the movable sever at the end of the structure (the use of a movable sever allowed the length of the structure to be varied without having to remove it from the electron stick). The gain which was measured involved the ratio of the powers at the end of the structure with and without the beam and so was a measure of the "intrinsic" gain of the structure, i.e., it did not involve the matches of any input or output couplers.

It was thought at first that the effect of the slots on gain could be measured by measuring the gain as a function of length and then comparing the asymptotic slopes of the curves thereby obtained, with and without external loading. However, such measurements produced inconsistent and inconclusive results. It is thought that the presence of the slots destroyed the asymptotic behavior of the tube gain. In fact, if the slot resonance were near the passband, one would expect rather large perturbations in the fields and propagation characteristics of the structure. If a sufficient length of unslotted sections were placed after the slotted sections, one would expect the tube gain to again approach an asymptotic value. However, this could not be checked for the structure first tested because of the

appearance of structure oscillations at relatively short lengths. The presence of spurious oscillation power completely confused the measurement of gain. It is planned to repeat the measurements of gain using a structure which is not so unstable, so that gains at longer structure lengths can be measured.

The effect of the slots on gain can also be determined by comparing the gains measured for a given length of structure which is loaded by the various suppression schemes. However, the gain of an unloaded structure which is long enough to include a sufficient number of slotted sections could not be measured for the first structure tested because of the appearance of structure oscillations. This gain, however, could be extrapolated from the asymptotic gains measured for shorter lengths. A comparison of the gains measured with slot loading with this extrapolated gain indicates that the various loading schemes reduce the gain away from beam-circuit synchronism much more than at synchronism. The correctness of this conclusion will be checked by repeating the gain measurements with a more stable structure This will allow the gain for longer lengths of unloaded structure to be measured. The effect of off-synchronism gain reduction is not understood as yet, but several possible theoretical explanations are being investigated. Also, since the slots are near resonance in the frequency range of interest, the reduction in gain must be considered in the light of the possible effects of the slots on the structure fields, propagation characteristics, and internal reflections. Additional experiments will be carried out in an attempt to determine these effects. Until these experiments are completed, no definite conclusions can be drawn concerning the effects of the slots on tube performance.

2. Theoretical Work

The theoretical portion of this study was directed toward understanding the oscillatory behavior of a periodic circuit near cutoff and deriving, if possible, a simple criterion for estimating the start-oscillation length at cutoff of a structure which has been loaded in various ways. At first, an attempt was made to describe the beam-circuit interaction at a cutoff by coupled propagating-mode theory, which provides a simple, semi-quantitative analysis of the gain and oscillation behavior of a high-power TWT for frequencies within a passband. However, it was soon determined that such

a theory could not be applied consistently at a cutoff unless the problem were solved exactly, which, in general, is not possible. Fortunately, an alternate approach using resonant modes is possible because the fields in the structure take on a resonant character at a structure cutoff. If one considers the structure to be composed of coupled cavities and does a perturbation analysis using the mode which is resonant at the cutoff frequency of interest, he obtains a theory which adequately describes the behavior of the system in a narrow frequency band around that cutoff. Away from cutoff the theory gives the same results as coupled-mode theory. Analyses of this type have been performed using equivalent circuits[1],[2] to describe the structure but were limited to identical cavities having identical losses so that solutions could be obtained in the form of waves. However, numerical methods must be resorted to in any case and we prefer to leave the theory general enough to cover the case where the losses in each cavity are not identical or even where the cavity resonant frequency and/or length are "tapered." The problem is then solved by the straightforward evaluation of certain matrices which appear in the theory. This theory has the additional advantage over previous theories in that the practicability and physical picture are improved because of the formulation in terms of well-understood and, for the moment, easily measurable cavity and beam parameters. In particular, the physical picture of the energy interchange between each cavity and the beam is quite clear.

The start-oscillation conditions for a structure having parameters equal to those measured for the first experimental structure (and beam) were found from this coupled-cavity theory and these agreed quite well with the start-oscillation conditions obtained experimentally, thus verifying the correctness of the theory to some extent. These results can also be compared with the start-oscillation length which is found from Wessel-Berg's Monotron Theory, for oscillations which occur at the cutoff frequency. This theory assumes that the whole structure at cutoff can be thought of as a single resonator, and hence the starting conditions are given by a

---

[1] R. W. Gould, Trans. IRE, PGED, ED-5, 186-195 (July 1958).

[2] D. G. Dow, Trans. IRE, PGED, ED-7, 123-131 (July 1960).

single, simple equation. However, because of the drift spaces between cavities, the Monotron Theory will always underestimate the starting length (current) and this is verified by comparison with the coupled-cavity theory. It can be shown that the beam comes close to giving up the maximum amount of power to the structure that it can when the field distribution in the structure is sinusoidal and the slow space-charge wave on the beam has the same phase shift per cavity as the structure fields. These conditions determine the minimum start-oscillation length at cutoff. In this case, Wessel-Berg's start-oscillation equation becomes:

$$n_{min} = \frac{\frac{1}{Q_0}}{\frac{L}{\ell'}\left(\frac{R_{sh}}{Q}\right)\frac{1}{4W}} \left(1 + \sqrt{1 + Q_0^2\left(\frac{1}{Q_{ext_1}} + \frac{1}{Q_{ext_n}}\right)\frac{L}{\ell'}\left(\frac{R_{sh}}{Q}\right)\frac{1}{2W}}\right),$$

where

n = number of cavities in the structure,

Q_0 = unloaded Q of a single cavity,

R_{sh}/Q = interaction parameter for a single cavity,

L = periodic length of the structure,

ℓ' = gap length of a cavity,

Q_{ext_1}, Q_{ext_n} = external Q's representing loading produced by couplers in the end cavities, and

W = beam impedance

$= 2\beta_q V_0/\beta_e I_0$.

Thus, if one only needs an estimate of the starting length at cutoff he can avoid the large amount of numerical work required by the coupled-cavity theory and use the above equation.

This will be considered in more detail, as well as the results of the more general theory, in a comprehensive technical report of this study now in preparation.

II. CENTIPEDE TWT

A. INTRODUCTION

The objective of this project is to study the electron beam-slow wave circuit interaction in a high power traveling-wave tube. The centipede slow wave structure has proven to be one of the most satisfactory structures for a high power TWT and will be used in this study [1] [2] The method of investigation will be to measure the amplitude and phase of the cavity fields of the centipede while it is mounted on the electron stick and is being operated as a TWT. These measurements in conjunction with a suitable equivalent circuit for the centipede will be used to calculate the amplitude and phase of the rf beam current in each centipede cavity. Since the equations relating the structure field quantities are inherently linear the beam current can be found under both small and large signal conditions.

The results of this study will be of utmost value in optimizing the many parameters affecting the beam-circuit interaction. Measurements of amplitude and phase over a particular region will be possible, such as at a sever and in the output section of a tube. It is hoped that insight gained from this study will make possible high power traveling wave tubes of higher efficiency and greater saturated bandwidth.

B. DISCUSSION

1. Experimental Progress

The fields inside each centipede cavity are sampled by a small, movable loop probe which is coupled to the fields by small rectangular slots located between the feed of adjacent centipede loops, as shown in Fig. 2.1. The

---

[1] M. Chodorow, A. F. Pearce and D. K. Winslow, "The Centipede High-Power Traveling-Wave Tube," Microwave Laboratory Report No. 695, Stanford University (May 1960).

[2] Third Annual Report for Contract AF 30(602)-1844, "The Centipede High-Power TWT," Microwave Laboratory Report No. 854, Stanford University (August 1961).

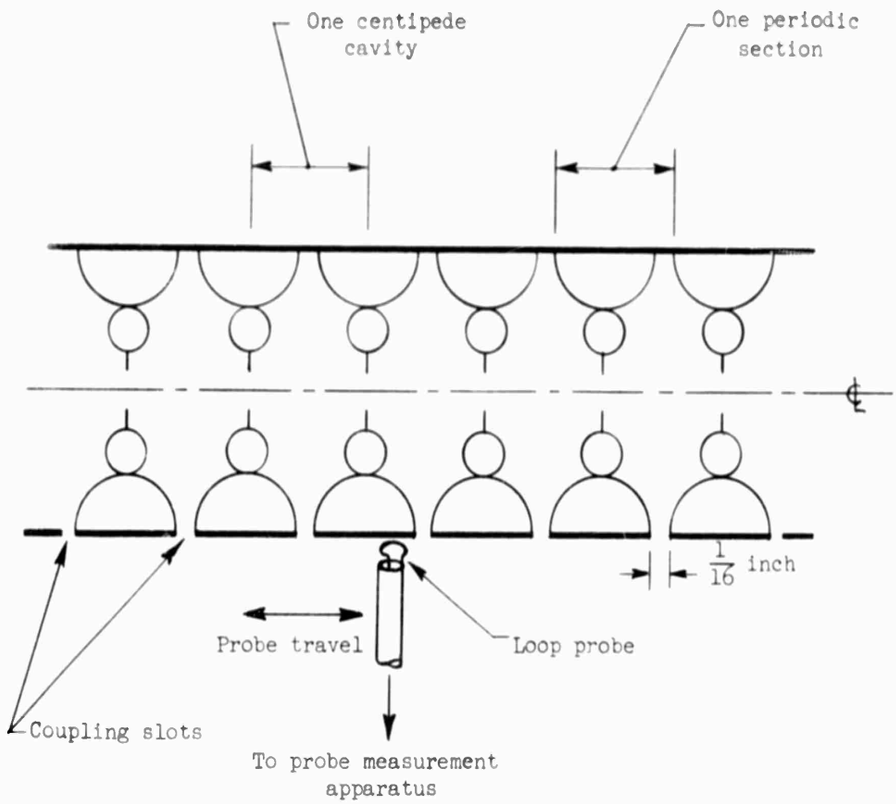

FIG. 2.1--Cross-sectional view of the centipede structure showing field probe and coupling slot location.

probe is attached to a mechanical apparatus which allows the probe to move over the entire length of the centipede structure and which allows precise positioning of the probe over any cavity slot. The slots, which are 5/16 by 1/16 in., were adjusted by trial and error so that one kilowatt of power at the centipede input coupler provides about one milliwatt of probe output when the probe is located over one of the slots close to the input. The fact that the coupling factor of centipede input to probe output is in the order of 10^{-6} means that the slots are too small to cause a noticeable perturbation of the centipede fields. Measurements have shown that probe output between slots is less than 10 μw.

The amplitude of the fields in each centipede cavity can be measured by positioning the movable probe over the coupling slot in a particular cavity and by using a crystal detector to measure the probe output. Since the centipede fields are pulsed, a peak reading voltmeter was built which gives a dc output proportional to the peak of the pulse. The apparatus that controls the position of the probe is motorized so that the probe can be made to sweep over all of the cavity slots quickly, producing a slot amplitude pattern. This pattern is thus a periodic sampling of the amplitude of the centipede field over the beam-circuit interaction length.

An initial cold test experiment was set up to test this measurement apparatus. The centipede was assembled with the traveling probe, a standard input coupler, a carbonized ceramic sever for a load, and a dummy section of electron stick placed on the axis. Assuming that the coupling coefficients of all the slots are the same, and that the structure has loss, the slot amplitude pattern for a reflectionless sever should be a decaying exponential curve as shown in Fig. 2.2. The centipede loops have been sprayed with Kanthal and the resultant fundamental passband attenuation is about 1/2 db/section at $\beta L = \pi/2$. Accordingly, the exponential decay in Fig. 2.2 corresponds to 1/2 db/section. However, the measured slot amplitude pattern showed that objectionable standing waves existed in the slow-wave structure terminated by a sever. Figure 2.3 shows a typical amplitude pattern near $\beta L = \pi/2$. While the pattern is regular and certainly indicates that standing waves are present, it is impossible to tell how much variation exists in the slot coupling coefficients. Since

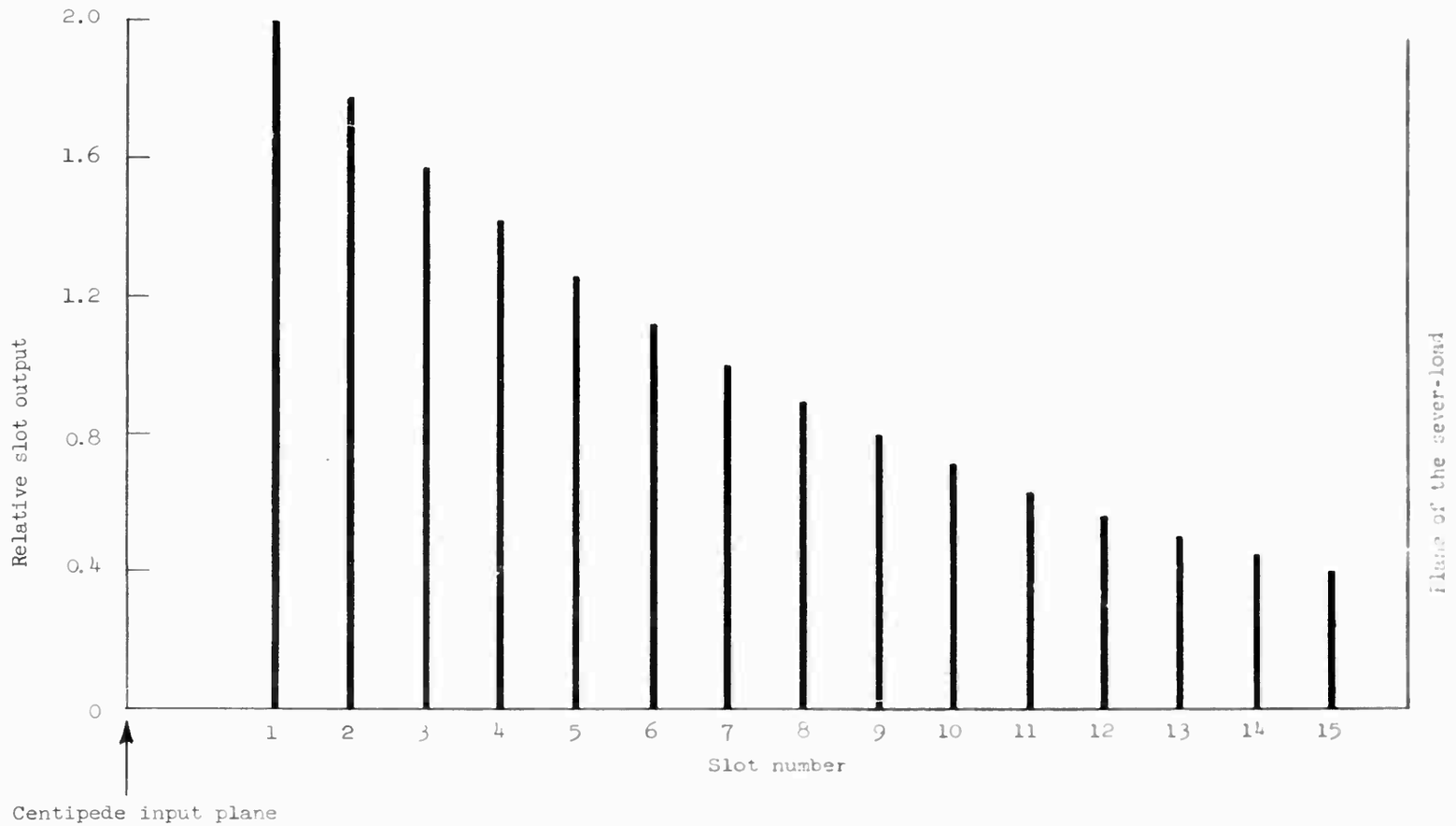

FIG. 2.2--Slot amplitude pattern for a reflectionless sever (0.5 db/section attenuation assumed).

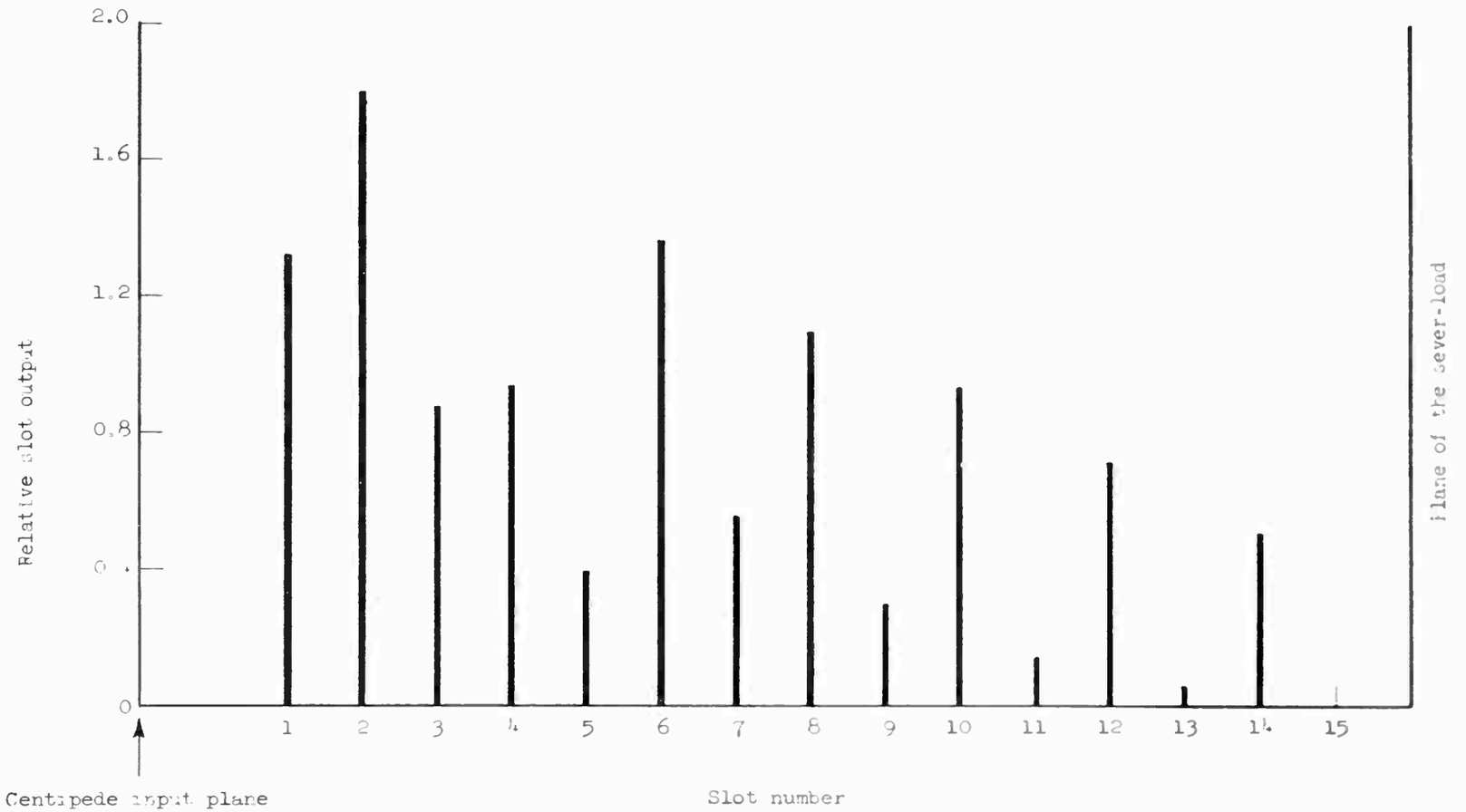

FIG. 2 3--Typical slot amplitude pattern (from experimental measurement at $\beta L = \frac{\pi}{2}$).

the reflection coefficient at the sever is unknown, it is difficult to calculate the theoretical amplitude pattern from transmission line theory.

One solution to the above problem is to replace the sever with a shorting plane, making sure that the short coincides with a centipede plane of symmetry. Then, if a square-law detector is used with the traveling probe, the detector voltage output can easily be found to be

$$\frac{V(n)}{V_0} = \frac{\cosh 2\alpha(N + 1 - n) + \cos 2\beta(N + 1 - n)}{2} , \qquad (2.1)$$

where

N = the total number of slots,

n = 1, 2, , N(n is the slot number, and the slots are numbered consecutively from the input). Note that slot N is one periodic length away from the short.

As shown in Fig. 2.4, experimental slot amplitude patterns have shown good agreement with Eq. (2.1) despite experimental errors of ± 5% in power measurement. The phase constant β in Eq. (2.1) was made equal to $\pi/2$ radians/section, and α was adjusted so that experimental and computed amplitudes were the same at slots 6 and 7. A comparison of the measured and computed amplitudes in Fig. 2.4 shows that the coupling coefficients of slots 4 and 14 are definitely lower than for the other slots.

A simple phase measurement technique has been devised to measure the phase of fields in one centipede cavity with respect to another. The microwave signal from the traveling probe is directed into one end of a waveguide slotted line, and a sample of the reference power driving the input of the centipede is applied to the other end. Phase of the fields in one cavity with respect to another is measured by observing the shift of a null in the slotted line as the traveling probe is moved from one slot to another. This is a relative phase measurement, and it allows the measurement of the large phase shifts seen between two adjacent cavities in the centipede. Phase shifts in range of $\pi/4$ to $3/4\pi$ are typical for normal TWT operation. Further information about this method can be found in the previous report [1]

---

[1] Quarterly Status Report No. 7 for Contract AF 30(602)-2575, Microwave Laboratory Report No. 1080, Stanford University (September 1963).

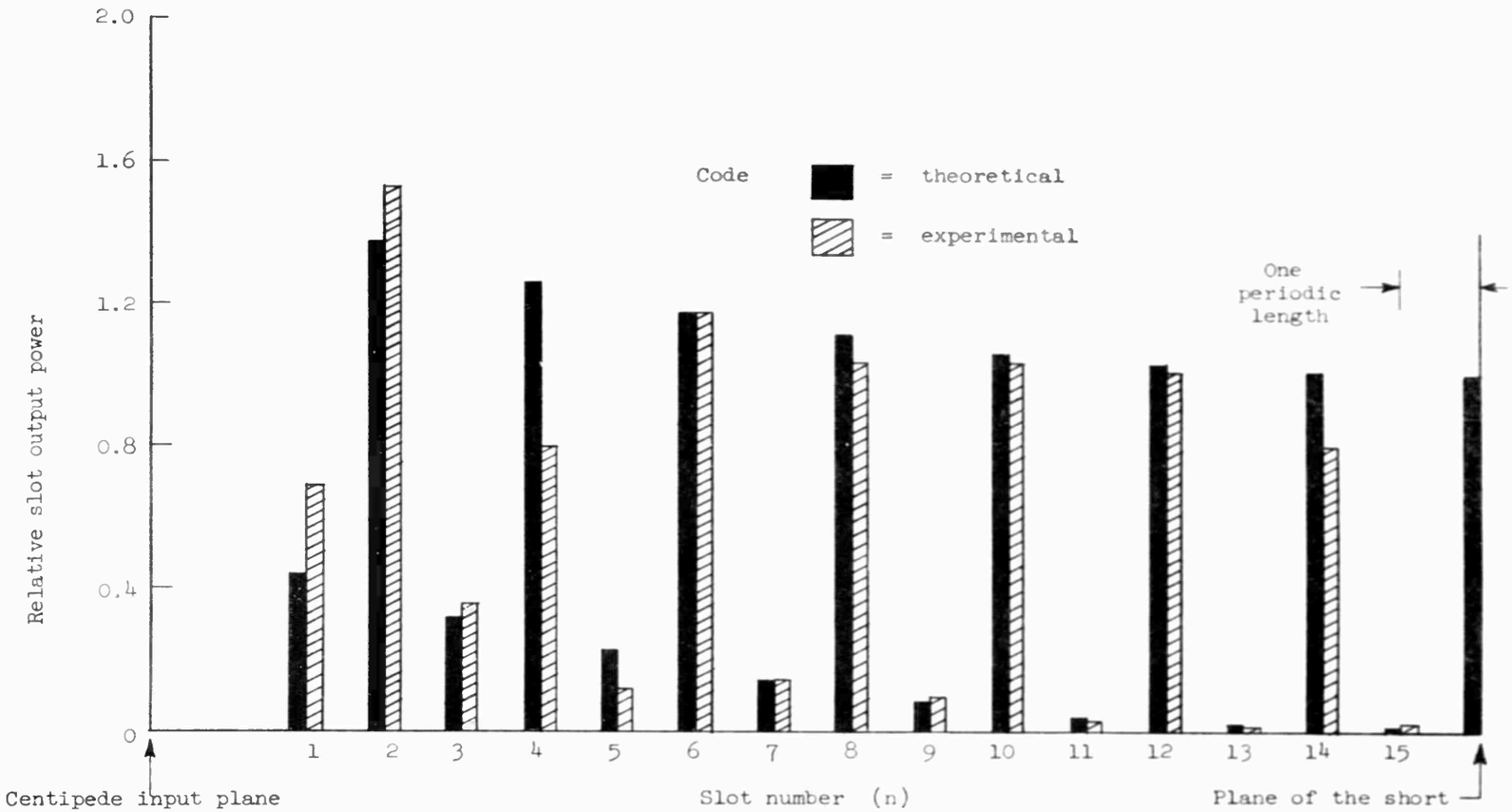

FIG. 2.4--A comparison of theoretical and experimental slot amplitudes ($\beta = \frac{\pi}{2}$ rad/section; $\alpha = 0.36$ db/section).

c Theoretical Progress

One of the goals of the past year has been to find a circuit model to represent the fields in each centipede cavity The circuit shown in Fig 2.5 is a representation of the centipede fundamental and loop modes. The negative mutual coupling of the centipede is accomplished in the circuit by crossing the wires, and the dispersion in the loop passband is approximated by the shunt tuned circuit L_2 , C_2 . Another tuned circuit, L_1 , C_1 , is related to the TM_{01} fundamental passband. The capacitance C_1 represents the effective electron beam gap in each cavity, while i_n is the effective rf beam current driving the nth cavity gap. Most important are the cavity voltage and current, V_n and I_n , since they are proportional to the cavity fields. With suitable adjustment of the element values, the circuit provides an excellent approximation of the centipede fundamental and loop passbands as is shown in Fig. 2.6. The circuit equations and the details of selecting the circuit values to match the centipede cold test data were given previously.(1) Since publication of this report, the circuit impedance of the circuit model has been found. The circuit impedance is defined as

$$K = \frac{V_n^2}{2(\beta L)^2 P} \quad , \tag{2.2}$$

where P is the power flow at the cavity gap,

$$P = \frac{1}{2} \operatorname{Re} V_n I_n^* \quad , \tag{2.3}$$

and βL is the phase shift per section. A straightforward analysis using the circuit equations and Eqs. (2.2) and (2.3) shows that the impedance is given by

$$K = (1/C_1) \frac{f_b^2 - f^2}{2\pi^2 k f^3 (\beta L)^2 \sin \beta L} \quad , \tag{2.4}$$

(1) Quarterly Status Report No. 6, Contract AF 30(602)-2575, Microwave Laboratory Report No. 1037, Stanford University (May 1963).

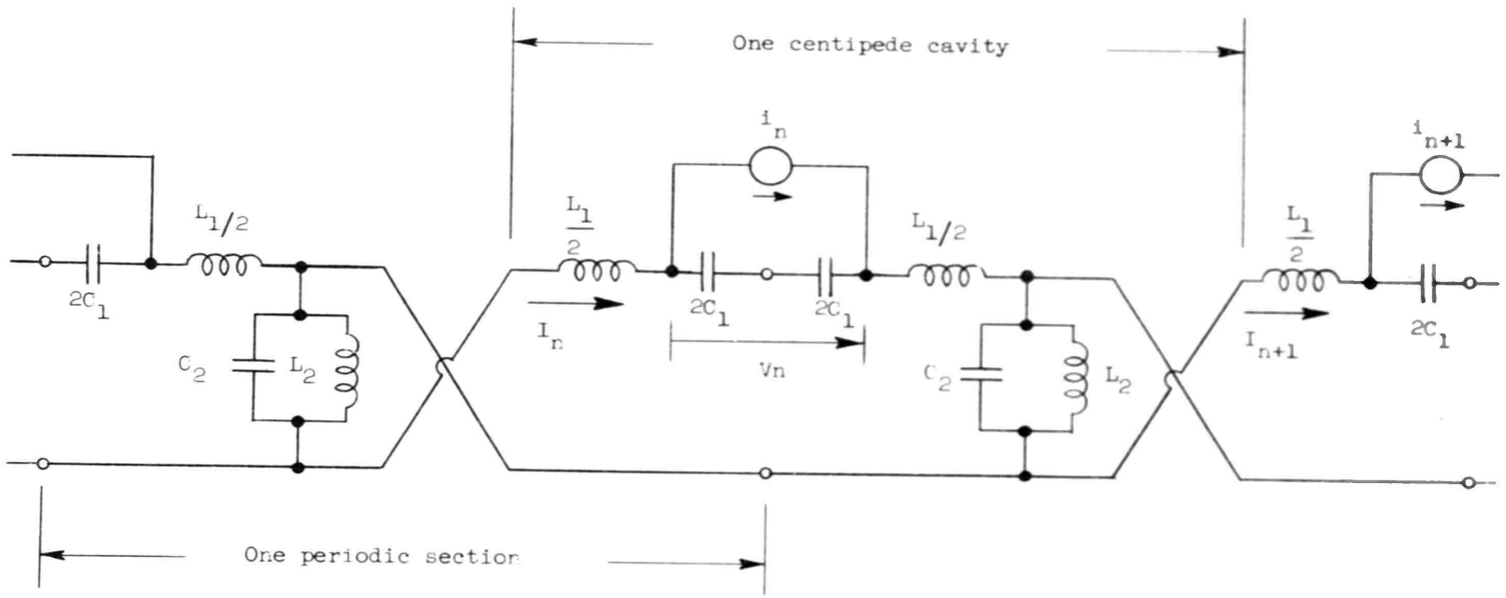

FIG. 2.5--Circuit model for the centipede TWT.

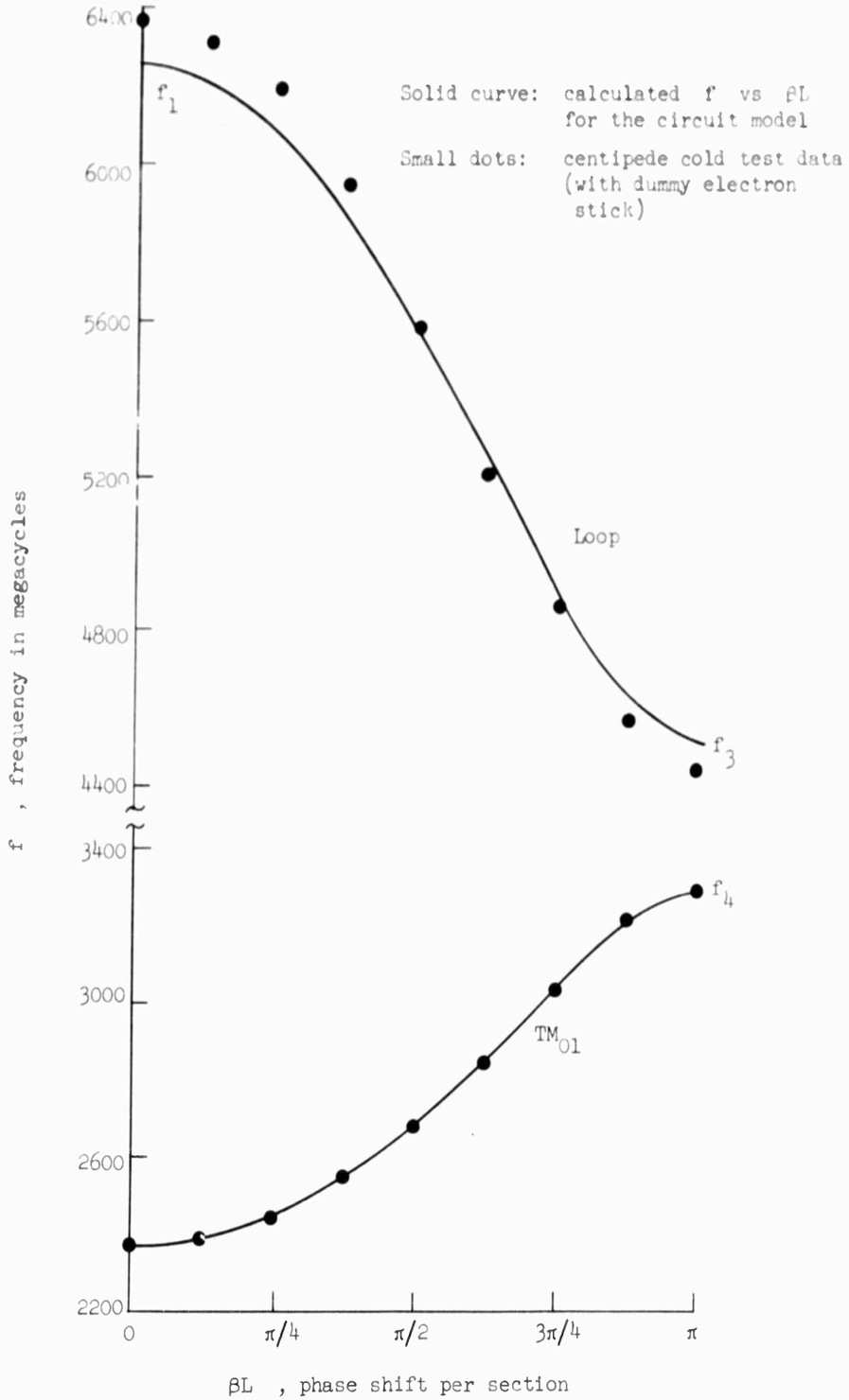

FIG. 2.6--A comparison of f vs βL for the centipede periodic circuit and its circuit model.

where

$$f_b = \frac{1}{2\pi L_2 C_2}$$

$$k = C_1/C_2 \quad .$$

The circuit quantities f_b and k were selected when the circuit was adjusted to match the centipede ω-β diagram. However, C_1 is still arbitrary so that the circuit impedance given by the model can be matched at one frequency to the experimentally found impedance vs frequency curve Figure 2.7 shows that reasonable agreement is obtained over the operating range of the centipede.

Another project completed this year was a small signal gain and phase computation for the centipede TWT using the analysis of Pierce.[1] The quantities x_1 and y_1 which are defined by Pierce and which are related to the gain and phase of the growing wave, were found using the curves of Brewer and Birdsall.[2] The asymptotic gain per section was computed for several beam voltages, and is shown in Fig 2.8. The calculated phase shift per section is shown in Fig. 2.9, along with the cold test ω-β diagram. While the Pierce theory has been shown to be inadequate at the passband edges,[3] a reasonable idea of the gain and phase near synchronism is obtained. In this region, the gain curves of Fig. 2.8 compare favorably with the small signal experimental data obtained earlier for one model of the centipede tube. For that tube the maximum gain was about 1.6 db/section, and though the corresponding gain computed here for the centipede mounted on the electron stick is about 1.3 db/section, the beam-circuit coupling has necessarily been reduced due to the intrusion of the glass tube surrounding the beam. The Pierce calculation will be used later as a comparison with another more complex calculation and with the experimental data that will be found for the centipede mounted on the electron stick.

---

(1) J. R. Pierce, Traveling Wave Tubes, D. Van Nostrand Co., Inc., New York, 1950, Chapters 7 and 8.

(2) G. R. Brewer and C. K. Birdsall, "Normalized Propagation Constants for a TWT for Finite Values of C ," Technical Memorandum No. 331, Hughes Aircraft Co., Culver City, California, (June 1955).

(3) R. W. Gould, "Characteristics of Traveling-Wave Tubes with Periodic Circuits," IRE, Trans. PGED (July 1958).

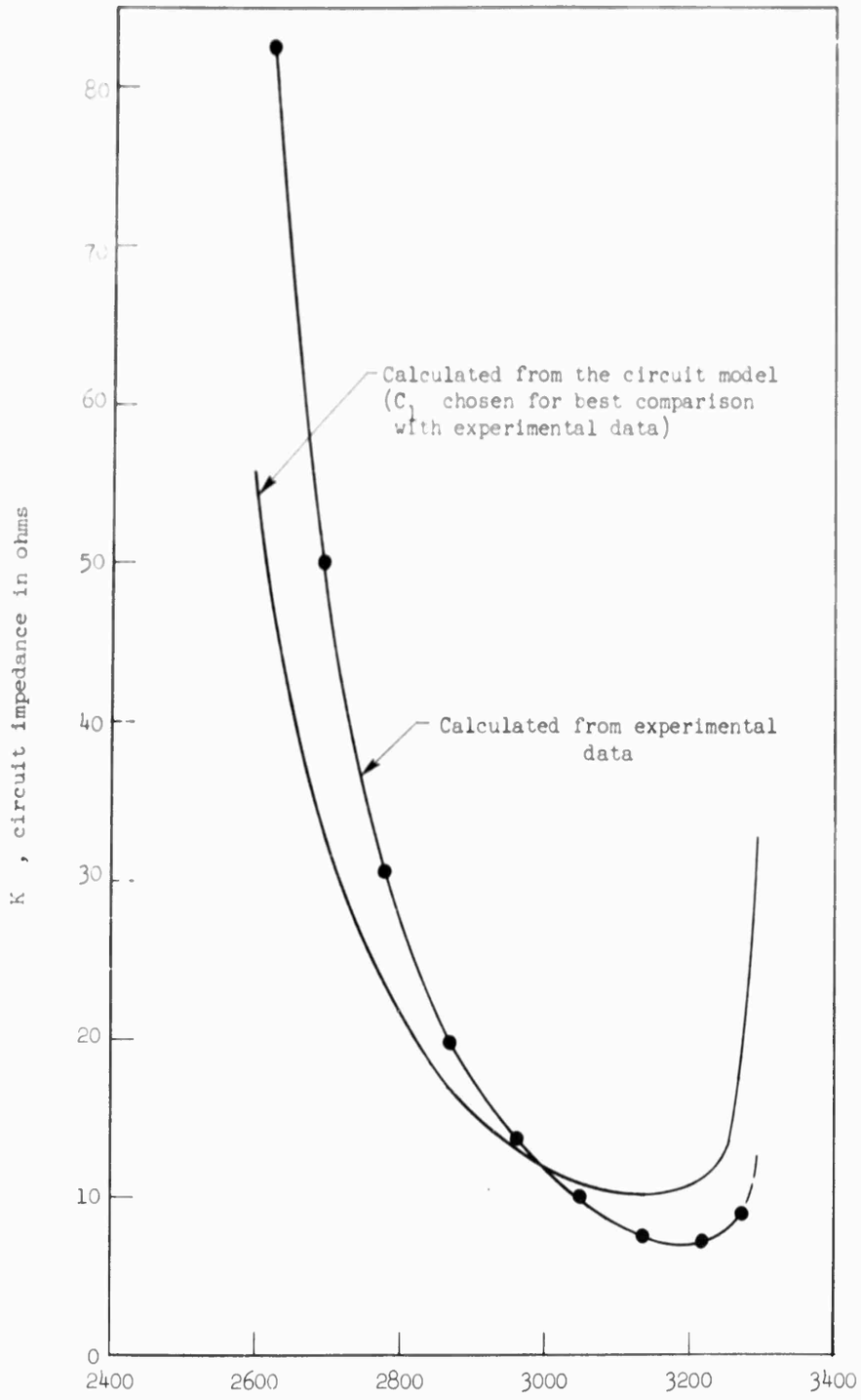

FIG. 2.7--Circuit impedance vs frequency.

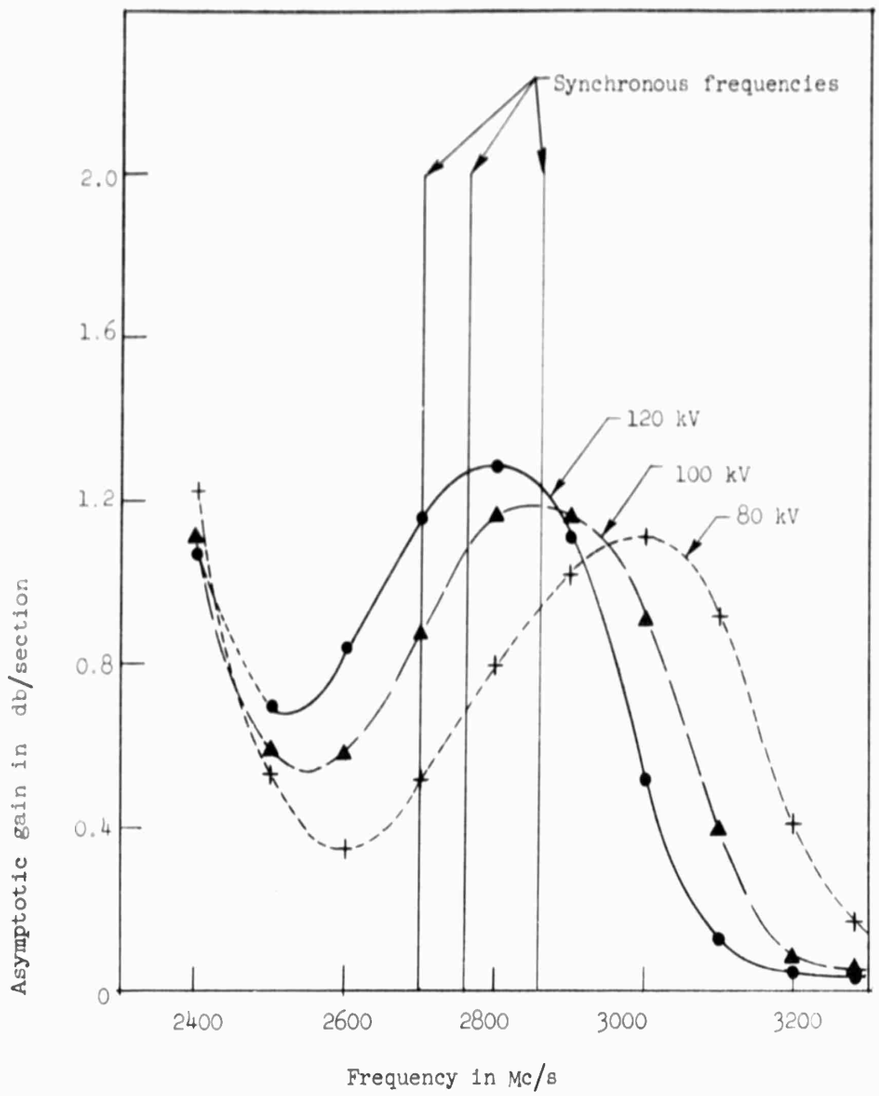

FIG. 2.8--Gain per section for the centipede TWT.

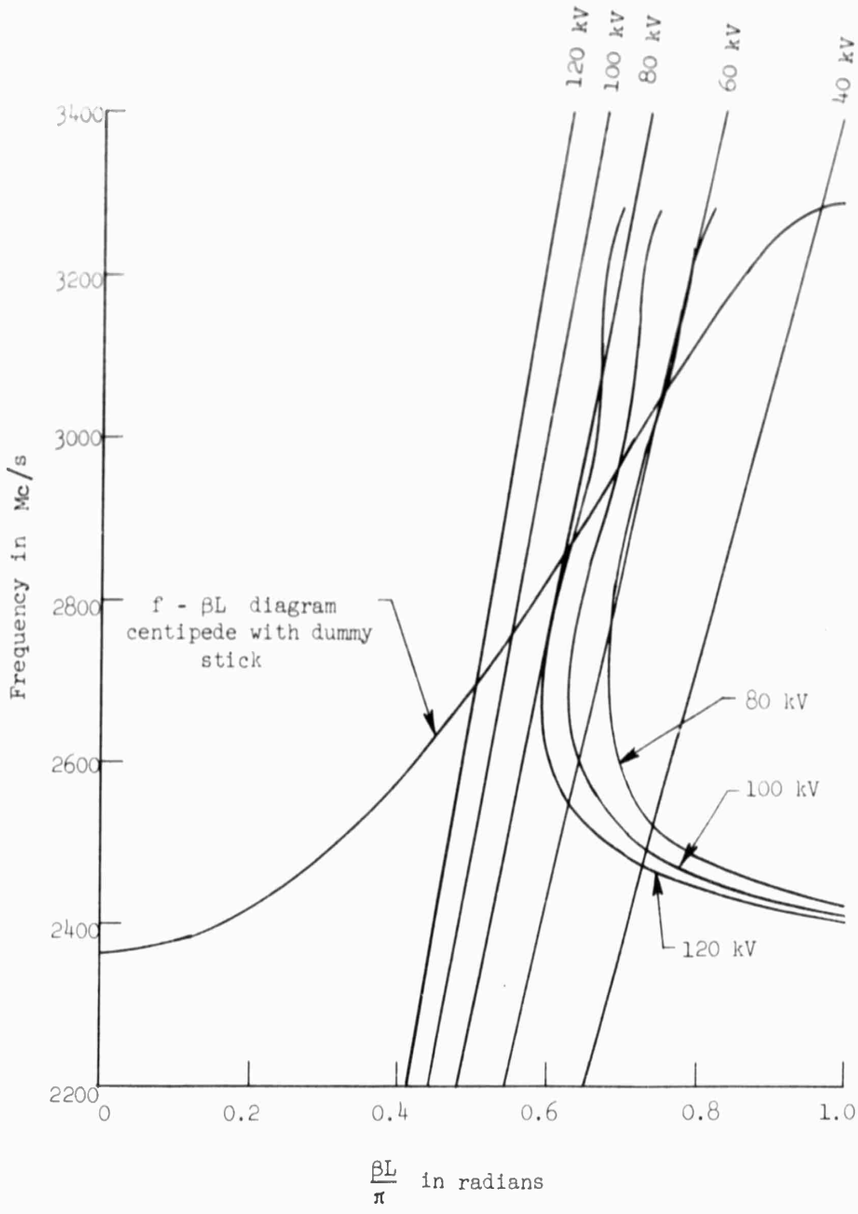

FIG. 2.9--ω - β diagram for the centipede TWT.

3. Future Plans

A small signal gain and phase calculation based on a paper by Gould[1] is now under way. This calculation includes the effect of two circuit and two electron beam waves and should give a better theoretical estimation of the centipede TWT operation. Since future phase measurements will require a good load for the centipede, a load made of several lossy centipede sections followed by the usual carbonized ceramic sever has been designed and will soon be cold tested Finally, gain and phase measurements will be made with the centipede operating as a traveling-wave tube. These measurements will be used in conjunction with the equivalent circuit described above to calculate the rf beam current along the beam-circuit interaction length.

[1] R. W. Gould, "Characteristics of Traveling-Wave Tubes with Periodic Circuits," IRE, Trans. PGED (July 1958).

III. LONG-SLOT TWT

A. INTRODUCTION

The objective of this project has been to investigate the long-slot traveling-wave tube which is capable of giving larger bandwidths than any of the megawatt tubes of this type and to improve its performance and stability characteristics. Tests on the first model of the long-slot coupled circuit TWT indicated its potentialities as a broadband, high-power amplifier with good electronic efficiency.[1] This first tube had, in addition to the upper passband oscillations and pulse-edge oscillations, a low frequency oscillation associated with the passband arising from the coupling slots. The long-slot circuit uses coupled cavities in which the coupling is accomplished through circumferential slots, resonant at a lower frequency than the fundamental forward wave operating passband. Work has been directed toward optimizing the circuit parameters to obtain good amplifier characteristics and toward the suppression of undesired modes to improve the stability of the amplifier.

A method has been devised to suppress the lower frequency slot-resonance mode, and cold test studies have been carried out, directed toward selectively loading the higher frequency modes. The loading scheme used for the higher frequencies consists of an external lossy waveguide which is coupled periodically to each cavity of the long-slot structure.[2] By adjusting the cutoff frequency of the attached waveguide and the resonant frequencies of the coupling slots to the external guide, not only can the upper modes be attenuated but also sufficient attenuation should be available to suppress the pulse-edge oscillations at the high frequency cutoff of the operating

---

[1] Second and Third Annual Reports for Contract AF 19(602)-1844), Microwave Laboratory Report Nos. 773 and 854, Stanford University, (January 1961 and February 1962).

[2] First Annual Report for Contract AF 30(602)-2575, Microwave Laboratory Report No. 987, Stanford University, (Nov. 1962). Note that this method is similar to that used in Part I of this report.

band. This type of attenuation is particularly attractive since at the operating frequencies of the tube, the attenuation is almost in a field-free region and thus imposes no power limitations on the tube.

During this contract year, a long-slot traveling-wave tube structure has been adapted for use on the electron stick as well as for continuing the cold test evaluation of the attenuation provided by the lossy external waveguides. Also an initial set of experiments has been performed on the electron stick for different lengths of structure with and without kanthal attenuation and with different slot lengths. The electron stick is certainly a valuable instrument for evaluating the stability characteristics of a structure when operating as a tube. For example, oscillations were observed at a frequency corresponding to the lower frequency slot mode with nine cavities with coupling slots of one length. However no oscillations were observed in this mode when the structure length was increased to as many as thirty cavities which had kanthal loss and with an appropriate staggering of slot lengths. The details of this and other measurements are presented in the discussion below.

B. DISCUSSION

The work during the past year has been directed toward the evaluation of the methods of suppression of the unwanted modes of the long-slot structure when operating as a tube on the electron stick. The cold test evaluation of the attenuation provided by an external lossy waveguide coupled to each cavity of the structure through resonant coupling slots, has been reported.[1] Next, the long-slot structure, with an appropriate input coupler, sever, and probe for sampling power for relative gain measurements, was adapted to and constructed for use on the electron stick. These cold tests were made with the electron stick in position so that measurements made on the stick would be consistent with the cold test results. The input standing-wave ratio of the coupler-sever combination was better than 2 to 1 throughout the operating passband. A number of sections were shorted in the usual way and the ω-β diagram with and

---

[1] Quarterly Status Report No. 5 for Contract AF 30(602)-2575, Microwave Laboratory Report No. 1012, Stanford University, (March 1963).

without the electron stick is shown in Fig. 3.1. Since one of the structures is composed of sections with slots of different lengths, the ω-β diagram for a number of sections with all long slots or all short slots is shown with and without the electron stick.

Different combinations of structures were then mounted on the electron stick in order to observe the effect of these combinations on the stability. The structure combinations used were the following:

(a) a structure composed of two disks with long slots followed by two disks with short slots, two long, two short, etc., with two long slot disks at both the coupler and sever with kanthal loss on the disks only;

(b) structure as in (a) except with no kanthal loss;

(c) structure with long slots only.

The length of all the structures could be easily changed on the electron stick. Except for the size of the drift tube which has been increased from three-quarters of an inch to seven-eights of an inch, and the perturbation of the electron stick, the structure used here is the same as that used in the previous tube.[1] This allows comparison between the observations here on the electron stick and observations of previous measurements on the completed tube. This comparison is given in Table 3.I. In general, this table illustrates that under certain conditions the oscillations observed with the electron stick have approximately the same frequency as those of the previously completed tube. Shown in Table 3.I are typical frequencies, the lengths, the structure combination, and the starting voltage of the oscillations. For example, with the long-slot sections only, (c) above, nine sections had start oscillations at 69 kV, but when the structure was mixed as in (b), the length was increased to 13 sections, starting at 72 kV with the observed frequency of 2808 Mc/sec. Note that this frequency is approximately twice that of the lower frequency, 1414 Mc/sec, and it is not clear why this frequency was observed as the oscillation frequency. Note that as the voltage increased to 88 kV, still

---

[1] Second and Third Annual Reports for Contract AF 19(602)-1844, op. cit.

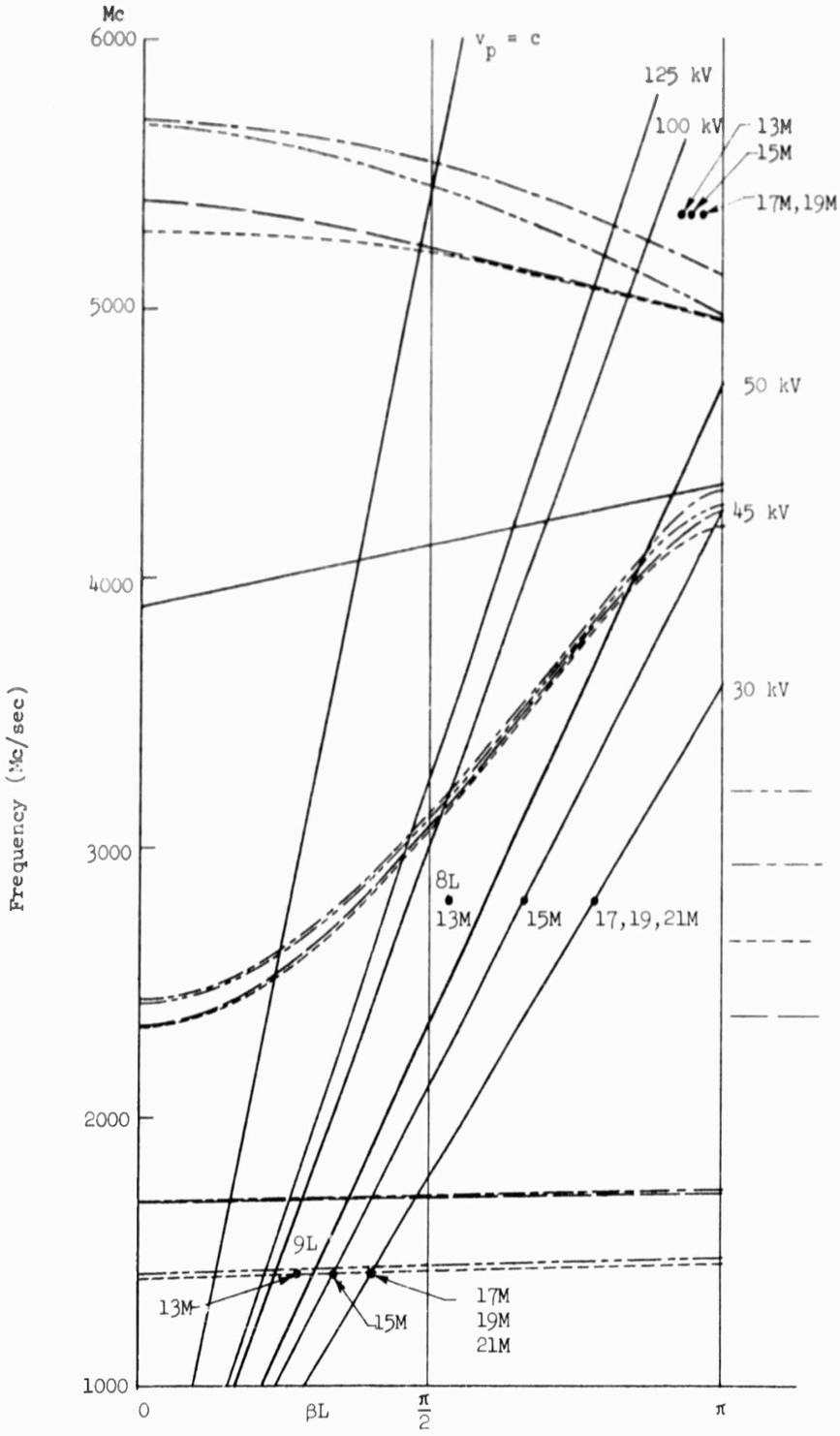

FIG. 3.1-- ω - β dispersion curve of the long-slot structure with long and short slots with and without the electron stick.

TABLE 3.I

FREQUENCIES OF OBSERVED OSCILLATIONS IN THE LONG-SLOT STRUCTURE

Tube I[1]		Electron Stick	
Frequency (Mc/sec)	Remarks	Frequency (Mc/sec)	Remarks
1490	Slot mode frequency	1414	Long-slot sections only 9 sections starting at 69 kV
2980	Begins at 40 kV multiple of 1490 Mc/sec	2808	Long-slot only 8 sections starting at 73 kV
3040	Intermittent		
4470	Disappears above 120 kV	2808	Mixed structure 15 sections starting at 72 kV
5440-5470	Higher mode oscillations	5340	Mixed structure 17 sections starting at 88 kV

(1) Ibid.

with 13 sections, that the 5340 Mc/sec oscillation takes over and is the stronger of the oscillations at the increased voltage. It is interesting and informative to plot the voltage and frequency at the start of oscillations for different numbers of sections of different types as in (b), and (c) above on the ω-β diagram shown in Fig. 3.1. Shown on the graph are the lengths of structures and voltages at which the oscillation started. At approximately 2800 megacycles are plotted the oscillations observed with mixed structures, composed of 13, 15, 17, etc., sections. The length is the number of sections in that structure. Then in the 5340 Mc/sec region, the TM_{02} of the structure is causing the oscillations. Note that as the structure length is decreased, the voltage at which oscillations are observed increases. Again, the oscillations observed at about 2800 Mc cannot be explained since no mode has been observed in cold test measurements. Hence the oscillations at the 2800 frequency region have also been placed on the graph at approximately half this frequency, at 1400 megacycles, and are so labeled 13 M, 15 M, 17 M, 19 M and 21 M, in (b) above. The observation was made of a mixed structure 30 sections long with kanthal on the disks and no oscillations at any voltage up to 90 kV were observed. The limiting voltage of 90 kV was the voltage at which stick oscillations began and affected the measurements for higher voltages. The attenuation due to kanthal disks was about 0.1 to 0.2 db per period and so should not degrade the overall characteristics of the tube appreciably. It is further to be noted here that oscillations at the cutoff frequency of the operating band at approximately 4200 Mc/sec were not observed. These oscillations would probably have been observed if other modes had been suppressed. The measurements of gain by means of a probe located in the sever were not successful. For this, the power was measured at the probe with the beam on and the beam off at the same drive power. These measurements were inconsistent in two different ways. First, the output power did not increase as the input power was increased and second, an increase in length did not give a corresponding increase in gain. This probe was moved to several different positions in the sever with no improvement in the consistency of the measurements.

In summary, a number of measurements have been made on the stability characteristics of the long slot TWT. The shortest length at which oscillations were observed was with 8 sections, all of the same slot length as in (c), above. These were in the lower slot mode at about 1400 Mc/sec beginning at about 70 kV. With a mixed structure, as in (b) above, 13 sections were needed at that voltage for the beginning of oscillations. However, with kanthal disks no oscillations were observed to 90 kV. Further work will include the mounting of the external waveguide to control the stability of the tube at higher frequencies, namely the 5350 Mc/sec, and the upper cutoff of the operating band. Gain measurements to evaluate the effect of the attenuation schemes should also be included.

IV. NONPERIODIC DIELECTRIC-LINED TRAVELING-WAVE TUBES

A. INTRODUCTION

The main concern of this project is the potentialities of high voltage (order of 100 kV) traveling-wave and related (e.g., distributed-interaction klystron) tubes whose rf structures are simply uniform, homogeneous sleeves of dielectric inside a copper shell. The high voltage corresponds to dielectric constants less than 10 in such tube designs and when combined with modest bandwidths (not over 30%) close to the TM_{01}^{o} mode cutoff, the same high interaction impedance and gain obtainable with periodic structures is to be expected. In addition, the possibility of using high-thermal-conductivity beryllia ceramic as the dielectric should permit exceptionally high-power capacity at a given wavelength. What should make the nonperiodic structure especially superior, however, as compared with periodic structures, is the freedom from spurious oscillations due to π-modes, backward space-harmonic waves and nearby extra passbands.

B. PRESENT STATUS

After choosing an S-band structure design compatible with the standard beam optics, and theoretically and experimentally establishing its interaction impedance and bandwidth, as well as demonstrating the feasibility of input/output couplings to it, the crucial problem in a reduction to practice is getting the electron beam through the central tunnel in the dielectric. This problem is also the major concern of the electron stick (see Parts I, II, III and V of this report), and the continuation of dielectric-structure work was postponed pending the final outcome of the stick project.

The beam tunnel of the electron stick is lined with a 50 T.P.I. tungsten-wire helix, rather than a continuous resistive film, mainly because the helix does not significantly load or perturb the TM_{01}^{o}-type waves of

externally-applied rf structures, but also because of thermal considerations. However, the helix supports waves peculiar to itself such that spurious backward-wave oscillations arise over a wide range of beam voltages. Some configurations of resistance-coated Mylar washers stacked external to the stick were found to control these spurious oscillations, through dissipative loading, without excessive perturbation of most of the present periodic structures, but they would be incompatible with the proposed nonperiodic structures. The remaining alternative is to modify the helix wire itself, retaining a core of tungsten - or molybdenum - (as the only refractory metals with a sufficiently low dc resistivity and a thermal-dilatation match to a low-loss glass) under a skin of high rf-resistivity material, which, of course, "sees" the spurious helix wave but not the TM_{01}^{o} waves to which the helix is "transparent." As the skin coating, kanthal is ruled out because of its thickness, brittleness, and inclination to interfere with attachment to the glass wall. Electroplated iron is the remaining alternative, subject to its retention of a high magnetic permeability, which, rather than the modest resistivity, leads to reduced skin depth and high rf resistance.

After a long search, and unsuccessful attempts by another electrochemical facility, only the Sylvania plant in Towanda, Pennsylvania, was found both willing and able to supply the required (0.010 in. diam.) tungsten wire with an adherent iron plating. They did find, however, that a uniform coating could not be made less than 0.0005 in. thick (order of 50 skin depths). Various wire samples were made in the inner conductor of coaxial cavities such that Q_0 measurements yielded the information that the iron plating, as shipped, raised the rf resistance at 3 Gc/s tenfold ($\mu \sim 60$). The effect on this result of variously oriented steady magnetic fields of the magnitudes common to focusing solenoids was found to be negligible and ferromagnetic resonance was not encountered. As well as can be estimated from available B.W.O. theory, a tenfold increase in helix wire loss could raise the start-of-oscillation current 20- to 100-fold, assuming 800 to 1500 ohms to be the most likely value of K_t (transverse impedance) for the present helix excited as if virtually all the wave energy exists in the 28 to 49 turns-per-wavelength field configuration of the space harmonic responsible for the oscillations. (Corresponding wire-loss figures are 0.01-0.02 and 0.01-0.02 db/turn, with and without iron plating, respectively).

A new electron stick tube with a helix of the iron-clad wire has been completed and is now being activated. The additional annealing which accompanies tube processing should, if anything, further increase the μ of the iron. Difficulties were encountered when the excessive thickness of the iron introduced thermal-dilatation mismatch with the glass, but alteration of the temperature, etc., used in shrinking the glass onto the wire, yielded usable electron sticks. The wire is less intimately bonded to the glass than before, but the structure is acceptable for the present. If tests prove the spurious waves have been suppressed, attempts to modify the deposition of iron so as to interfere less with the glass shrinking will be justified.

Proof of oscillation control by the iron plating will also justify resumption of active design and hot testing of nonperiodic dielectric structures. Present thinking is that a resonated length of dielectric structure serving as the output cavity of a distributed-interaction klystron built around the new stick may yield hot data with the least construction effort. Plans for millimeter tubes (which must resort to the resistive-film type of tunnel lining that does attenuate TM_{01}^{o} waves) and investigation of anisotropic dielectrics (which are not yet available in usable form) were not actively pursued this year.

V. EXTENDED-INTERACTION KLYSTRONS

A INTRODUCTION

In the generation of microwave power at megawatt levels one is faced with the twofold problem of realizing a maximum of gain-bandwidth product while expending a minimum of costly dc energy, i.e., while achieving high conversion efficiency. As has been demonstrated by theory and experiment,[1],[2] extended-interaction klystrons, with cavities consisting of resonated sections of slow-wave structure, are highly satisfactory in both respects; it is the purpose of this project to further pursue the investigation of this type of tube. Our work has been mainly concerned with the search for a suitable high-velocity circuit, and the beam-testing of such a circuit, with the ultimate objective of designing a high-power klystron which realizes to the limit all the potential advantages of extended interaction. For convenience, the beam tests are being conducted by means of the electron stick described earlier. The electron stick is a 100 kV pulsed electron beam with a perveance of 2.0×10^{-6}, enclosed in a slender evacuated glass tube which can be inserted into the structure to be tested without any need for further evacuation. The great flexibility offered by such an arrangement is an obvious and important advantage over vacuum-enclosed systems; as might be expected, one pays a price for this in the form of some decisive design and operational constraints which are discussed below.

The theory predicts that the gain-bandwidth product of an extended-interaction klystron increases with the Pierce impedance of the resonated

---

[1] M. Chodorow, T. Wessel-Berg, "A High-efficiency Klystron with Distributed Interaction," IRE, Trans. PGED, ED-8, 44-55 (Jan. 1961).

[2] T. Wessel-Berg, "Space-charge Wave Theory of Interaction Gaps and Multi-cavity Klystrons with Extended Fields," NDRE Report No. 32, Norwegian Defense Research Establishment, Kjeller, Lillestrøm, Norway (Sept. 1960).

slow-wave structures. Consequently, the first part of our work was devoted to the investigation of planar-type structures which were known to have good interaction impedance. The results of this investigation have been described in detail.[1] However, the combination of the planar circuit with the circular-symmetric electron stick was seen to lead to a low interaction impedance at the beam due to the high average separation of beam and circuit; this separation reflects the misalliance of shape as well as the physical presence of the glass envelope surrounding the beam (e.g., at a frequency of 2.65 Gc and with an 80 kV beam one finds that near synchronism $\gamma a = 1.23$) . On the other hand, "shaping" the planar circuit to more nearly conform to the beam, and thus give higher impedance on the beam axis, led one consistently back to a stub-supported ring-bar structure, so that the latter circuit becomes an obvious choice for use on the electron stick. The detailed design of such a circuit has been given earlier.[2]

An operational problem is posed by the tendency of the electron stick to oscillate with the (-1) space harmonic of the thin-wire tungsten helix, whose role was included to prevent the inside of the glass tube from accumulating negative charge. Aside from the general undesirability of having a strong parasitic signal on the beam, particularly during small-signal measurements, it also turned out that the presence of the backward wave on the beam drastically reduces the backward insertion loss between cavities and thus encourages feedback instability, making klystron operation in the presence of these oscillations virtually impossible. To date, the only practical way to suppress the oscillations has been to stack resistance-coated Mylar washers, spaced by thin polyfoam washers, in available openings in the circuit under test. The use of an iron-plated tungsten helix which is presently being installed may eliminate the oscillation problem more efficiently, however. An adaptation of the Mylar-washer scheme to the stub-supported ring-bar circuit has been described.[3] Due to the close spacings of this circuit, loading of radial fields by the Mylar

---

[1] Microwave Laboratory Report No. 987, First Annual Report for Contract AF 30(602)-2575, Stanford University, (December 1963).

[2] Microwave Laboratory Report No. 1012, Quarterly Report No. 5 for Contract AF 30(602)-2575, Stanford University, (March 1963).

[3] Microwave Laboratory Report No. 1037, Quarterly Report No. 6 for Contract AF 30(602)-2575, Stanford University, (August 1963).

washers has been difficult to prevent. The arrangement used represents the heaviest ohmic and dielectric loading on the circuit which was still deemed tolerable, i.e., which still permitted the excitation of distinguishable longitudinal resonances in the cavity. On the other hand, this amount of loading provided to be insufficient to suppress the parasitic oscillation, at beam voltages of interest, when the loaded section of ring-bar structure exceeded a certain length.

The choice of S-band operation was a matter of convenience in using equipment readily available. Clearly the rapid decay of fields away from the circuit, at S-band frequencies, implies a sacrifice both in strength and in uniformity of the fields available for beam interaction. However, since the significant interaction parameter for a klystron cavity, M^2R_{sh}/Q , is proportional not only to the Pierce impedance of the resonated structure but also to its length, it was hoped that the loss in beam interaction due to field decay could be made up by using a longer interaction length, with monotron oscillations of the long cavity being prevented by heavy external loading. The final design of a coupler to permit the tightest possible coupling to the stub-supported ring-bar structure has also been described.(1)

Since bandwidth and efficiency in a multicavity klystron are mainly determined by the output cavity, it was decided, as a further expedient, to limit an initial experiment to the study of the demodulation of an appropriately bunched high-power beam by an extended-interaction output cavity. The desirable broadband bunching action of a stagger-tuned succession of input and intermediate cavities was, in effect, simulated by using two conventional narrow-band klystron cavities which are tunable so as to track the wide band of a heavily loaded output cavity.(2)

The complete experimental arrangement, then, consists of a tunable two-cavity input or bunching section, using simple re-entrant cavities, which is followed by a fixed-tuned, heavily-loaded, extended-interaction output cavity (Fig. 5.1) Beam tests with this arrangement have been completed during the last interval and are discussed in detail below.

---

(1) Microwave Laboratory Report No. 1037, Quarterly Report No. 6 for Contract AF 30(602)-2575, Stanford University, (August 1963).

(2) Microwave Laboratory Report No. 1012, Quarterly Report No. 5 for Contract AF 30(602)-2575, Stanford University, (March 1963).

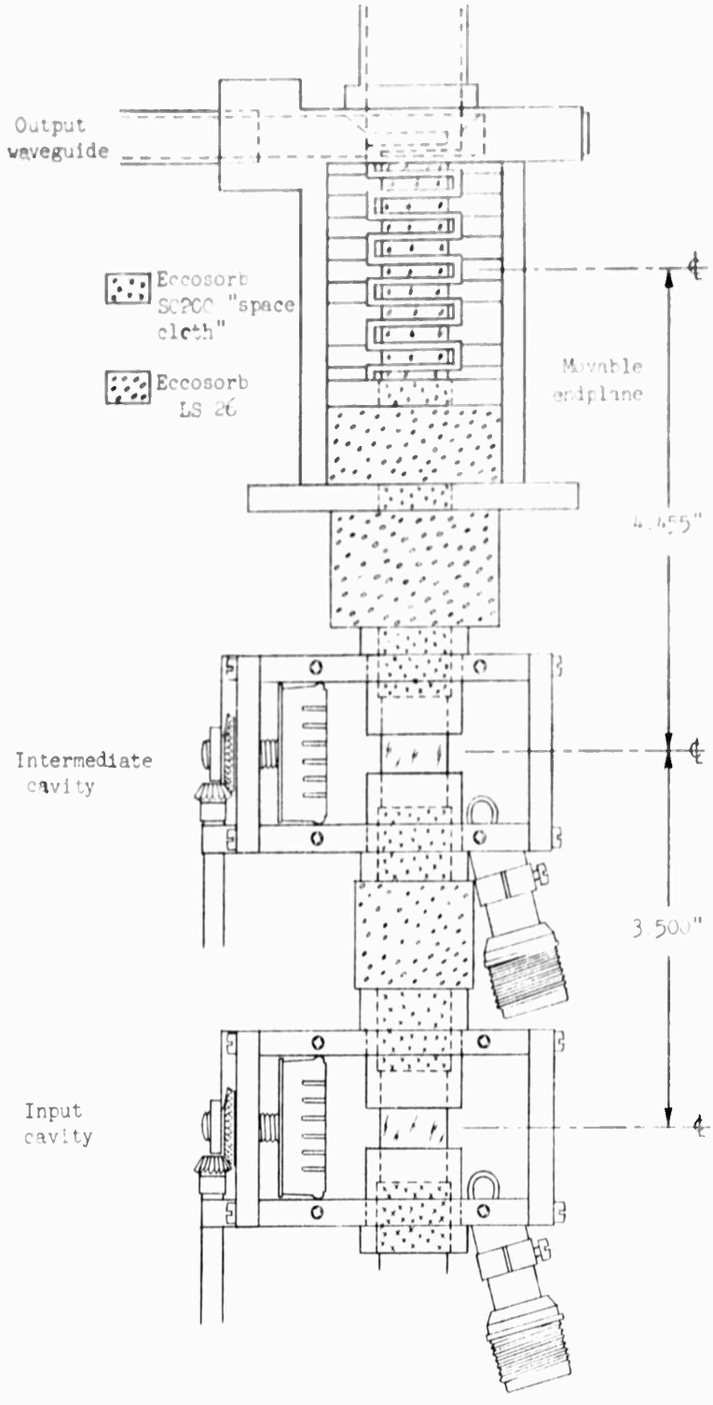

FIG. 5.1--S-band hybrid tube with output cavity masked down to L = 2π
(Mylar loading not shown)

B. DISCUSSION

1. Beam Tests of an S-band Hybrid Tube

a. Design parameters

The output cavity in its final form consists of a resonated three-inch section of stub-supported ring-bar structure, comprising a total of 15 rings or 7.5 periodic lengths. The cavity can be made shorter by use of a movable endplane. It is designed to operate, when placed on the electron stick, around a center frequency near 2.65 Gc, corresponding to a phase shift of 0.2π radians between successive rings. Phase velocity is $v_p/c = 0.45$ and group velocity is $v_g/c = 0.0365$. The normalized shunt impedance on the axis is $R_{sh}/Q_0 = 66.5$ ohms per resonant wavelength; this does not include any impedance reduction effected by loading the circuit with the resistance-coated Mylar washers, since impedance measurements cannot be made under heavily loaded conditions.

The input and intermediate cavities are basically identical to those used in the Stanford L 272 klystron, made tunable over the range 2.6 - 2 95 Gc by the addition of a tuning plunger. The R_{sh}/Q on the axis is 130 ohms; the transit angle at 80 kV and 2.65 Gc is $\beta_e D = 1.0$ radians.[1]

The drift tubes and the ring-bar circuit have an I.D. = 0.875 in.; for the latter, this implies $\gamma a \cong \beta_e a = 1.23$ at 2.65 Gc and 80 kV. The drift lengths are adjustable.

2. Measured Results

Initial beam tests involved an output resonator eight inches (four resonant wavelengths) long, but in these tests the amplified signal was found to be quite unstable in amplitude. The active length of the cavity was then reduced by means of the movable endplane, with the remaining length made inactive by wrapping the electron stick with lossy cloth. With this arrangement the signal did become stable; however, since the coupler end of the cavity had to remain active, only the gun end could be masked off, and thus the drift distance from the buncher section became

---

[1] This corresponds to a gap width of 0.34 in. The electron stick within the drift tubes was wrapped with Eccosoro SC 200 "space cloth" to suppress oscillations; the klystron gaps were centered over 1.05 in. long gaps in this wrapping. This arrangement resulted in $Q_0 \cong 600$ for both klystron cavities.

excessive. For this reason the output cavity was then permanently shortened, with electrical length now limited to a maximum of $\beta\ell = 3\pi$, at 2.65 Gc. In order to minimize feedback (see below) the drift-tube sections between cavities were completely removed and replaced by thick sleeves of lossy material (Eccosorb LS 26). The resultant assembly is shown in Fig. 5.1.

a. Gain measurements

With the output cavity adjusted for $\beta\ell = 2\pi$, the three-cavity synchronous gain at 80 kV is 19 db with a 3 db bandwidth of 3.5% (see Fig. 5.2). The two-cavity gain of the tunable bunching section, measured under the same loading conditions, remains constant, over the range of interest, at 11.0 ± 1.0 db. For simplicity, all cavities were critically coupled, with $Q_L = 55$ for the klystron cavities, and $Q_L = 35$ for the output cavity, including beam loading.

The three-cavity gain with the output cavity at $L = 3\pi$ was not measured because with this interaction length the system already became unstable. While it was thought at first that the instability was due to monotroning, i.e., to insufficient loading of the output cavity, it soon became evident that a feedback mechanism was involved which correlated strongly with the presence of parasitic oscillations on the stick. The extent of this correlation is illustrated in Fig. 5.3, showing total attenuation vs beam voltage, at 2.64 Gc, measured from the intermediate cavity towards the input cavity, i.e., looking backwards along the beam, with drift tubes replaced by Eccosorb sleeves. With the output region inactivated by lossy-cloth wrapping of the electron stick, one observes a gradual decrease of attenuation with beam voltage. This is due in part at least to lower reflection losses in both cavities as critical coupling (near 80 kV) is approached. Note that there are no parasitic oscillations in this case. With the output cavity operative, however, strong oscillations at 4.3 Gc are seen to begin near 68 kV, accompanied by a sudden 15 db drop in total attenuation of the backward signal. A closer investigation of the mechanism involved is beyond the scope of this work; its mere existence shows, however, that klystron operation on the electron stick is quite incompatible with the presence of parasitic oscillations.

The observed stability behavior of the three-cavity system is consistent with the phenomonon observed in Fig. 5.3: Strong parasitic oscillations

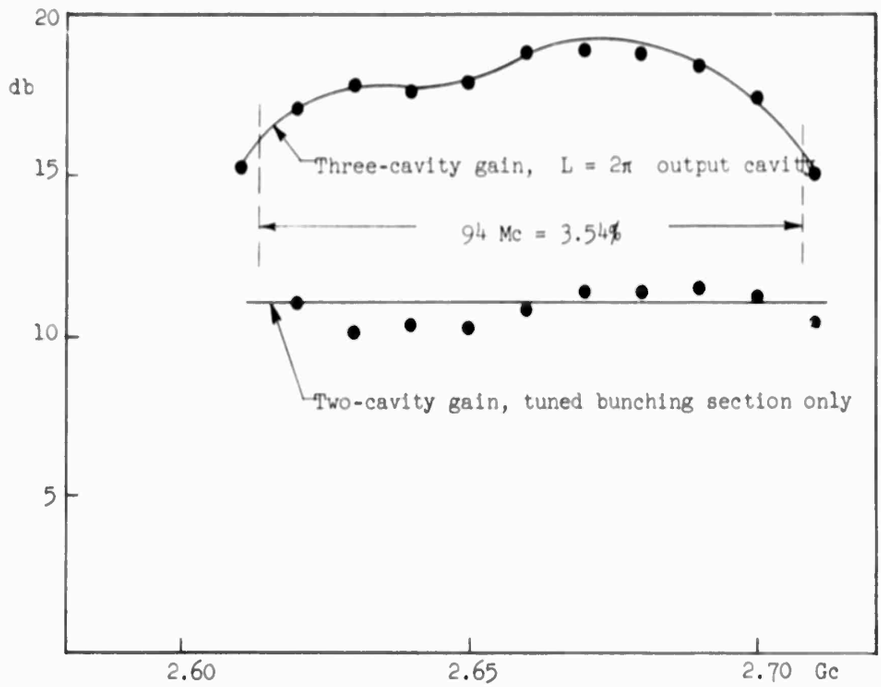

FIG. 5.2--Small-signal gain at 80 kV (bunching section tuned synchronously).

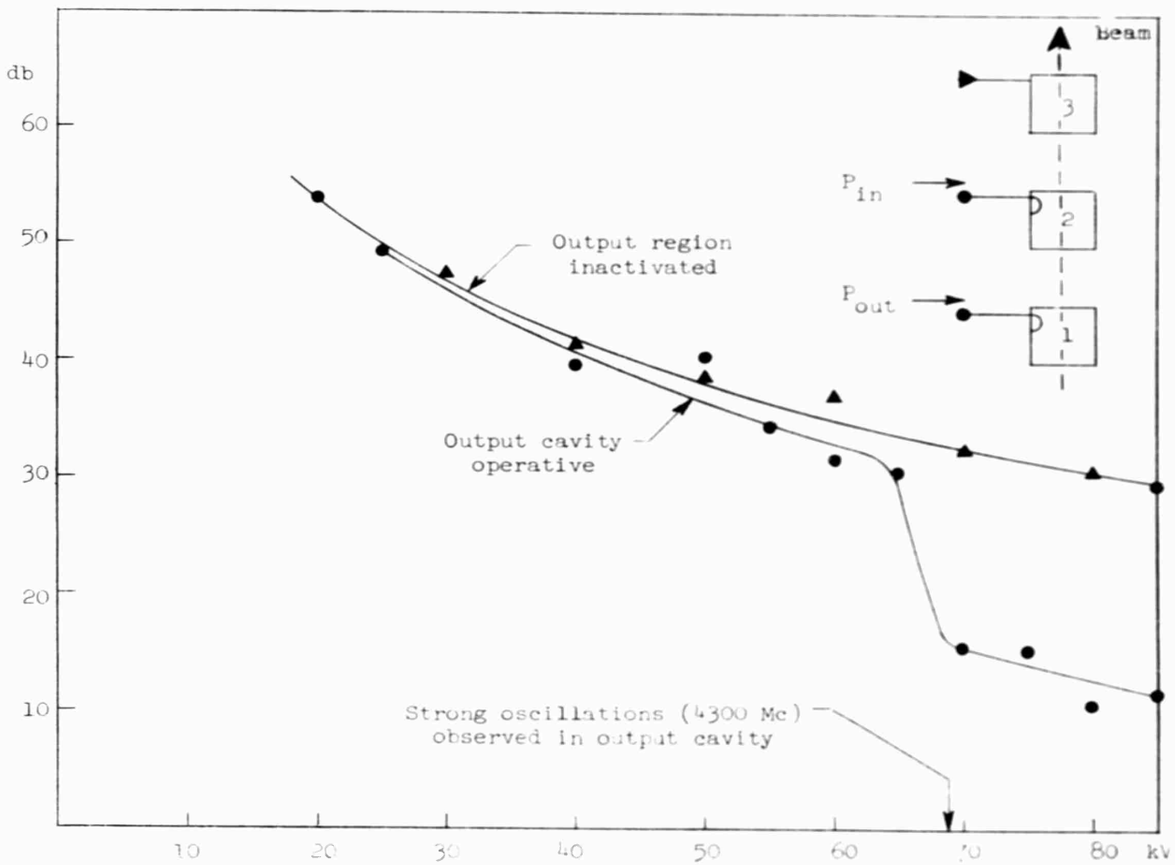

FIG. 5.3--Total attenuation at 2.64 Gc, from second to first cavity vs beam voltage (both cavities critically coupled at 80 kv)

begin near 40 kV for $\beta\ell = 3\pi$ but not until 85 kV for $\beta\ell = 2\pi$; hence stable gain at 80 kV could be expected for $\beta\ell = 2\pi$ but not for $\beta\ell = 3\pi$.

All measurements are small-signal; saturation measurements were precluded by arcing in the output cavity near the 30 kW level. At any one frequency, the bunching cavities were manually tuned to synchronism; the output cavity is, of course, fixed-tuned.

b. Beam loading measurements

A direct measure of beam-cavity interaction can be had from the evaluation of beam loading. Measured results are summarized in Table 5.I. In either of the two cases measured, beam loading was found to be less than predicted by the theory; however, the reason for this is not clear.

TABLE 5.I

NORMALIZED BEAM LOADING CONDUCTANCE, G_e/G_0 , MEASURED AT 80 kV

Cavity	Measured	Predicted
Buncher	0.116	0.175
Output with $L = 2\pi$	- 0.102	- 0.160

c. External loading of an extended-interaction cavity

As indicated before, the rationale behind this experiment was that although environmental conditions made it difficult to get high R_{sh}/Q per unit length on the beam axis, a large total R_{sh}/Q could be built up by using a sufficiently long section of slow-wave structure, with monotron instability of the resultant resonator being prevented by heavy, preferably external, loading. The fact that parasitic oscillations on the electron stick turned out to be the factor limiting maximum cavity length should, however, not obscure another more basic limitation on an arrangement of this type, concerning the external loading.

First, it is clear from the definition of Q_{ext} that for any cavity consisting of a resonated section of lossless transmission line, Q_{ext}

will be proportional to the length of the cavity. More explicitly, if the coupler reflects no power in either direction we may write, looking at the standing-wave pattern as a superposition of two waves,

$$Q_{ext}(\min) = \omega \frac{\text{energy stored}}{\text{power lost}} = \omega \frac{2 W_s \ell}{W_s v_g} = 2\beta\ell \frac{v_p}{v_g} , \quad (5.1)$$

where ω = radian frequency,

W_s = energy stored per unit length in one wave (incident or reflected)

ℓ = length of structure,

v_p = phase velocity, and

v_g = group velocity.

It is assumed throughout that the power flow in one wave can be correctly represented by

$$P = W_s v_g \quad . \quad (5.2)$$

For a lossy structure, Eq. (5.1) is modified slightly since there will be less energy stored, on the average, per unit length; power lost remains at its maximum, equal to incident power. For a transmission-line resonator with a given Q_0 one may then plot the lowest loaded $Q\ [Q_L(\min)]$, corresponding to maximum overcoupling as a function of resonant length $\beta\ell/\pi$.[1]

Secondly, from Wessel-Berg's theory,[2] one can find the maximum loaded $Q\ [Q_L(\max)]$ of a slow-wave resonator of given length, which will still prevent monotron instability when the resonator is made to interact with a given beam.

A simultaneous plot of $Q_L(\min)$ and $Q_L(\max)$ vs resonant length $\beta\ell/\pi$ will define a region in the Q_L - $\beta\ell/\pi$ plane in which operation of

---

[1] In our case, maximum overcoupling was approximated by designing for a smooth transition between the reduced-height waveguide and the slow-wave structure, with the latter temporarily terminated at the far end.

[2] T. Wessel-Berg, "Space-Charge Wave Theory of Interaction Gaps and Multi-cavity Klystrons with Extended Fields," op. cit.

a given slow-wave structure as a klystron resonator is practical. Such a plot has been drawn for the ring-bar structure used in this experiment (Fig. 5.4). One concludes from this plot that $\beta\ell = 3\pi$ represents the maximum interaction length which is not susceptible to monotron instability. However, with $R_{sh}/Q = 100$ ohms or $M^2 R_{sh}/Q = 50$ ohms, the $\beta\ell = 3\pi$ cavity clearly cannot satisfy the stated objective of relatively high total shunt impedance.

3 Summary of Results

The beam testing of a three-cavity hybrid tube on the electron stick has been completed. With the output resonator adjusted for interaction over one resonant wavelength, the overall small-signal gain was found to be 19 db with a 3 db bandwidth of 3.5%. Longer interaction lengths were made impractical both by parasitic oscillations on the electron stick and by the inherent difficulty of loading a long resonator sufficiently to prevent monotron instability. The two-cavity gain of the tunable bunching section remained at 11.0 ± 1.0 db over the frequency range of interest. Large-signal or saturation measurements were not made, due to arcing in the output resonator at the 30 kW level.

C. FUTURE WORK

It is evident from the above results that the realization of a stable slow-wave resonator with large total R_{sh}/Q at S-band frequencies, and built to be consistent with the electron-stick geometry, is fraught with considerable difficulty. Calculations show, however, that operation of the ring-bar circuit at L-band frequencies promises much better performance, with R_{sh}/Q in the order of 400 ohms per resonant wavelength, compared to 70 ohms for the S-band circuit. Work has begun on the design of a three-cavity L-band klystron, with all cavities consisting of resonated sections of ring-bar structure, and with the first two cavities again made tunable. For greater simplicity in design, no stub supports will be used on the ring-bar structure. With the tube designed to operate in the 20-30 kV range, it should be simpler to suppress parasitic oscillations on the electron stick. At the same time, saturation power levels will be lower and thus the chance of arcing will be reduced.

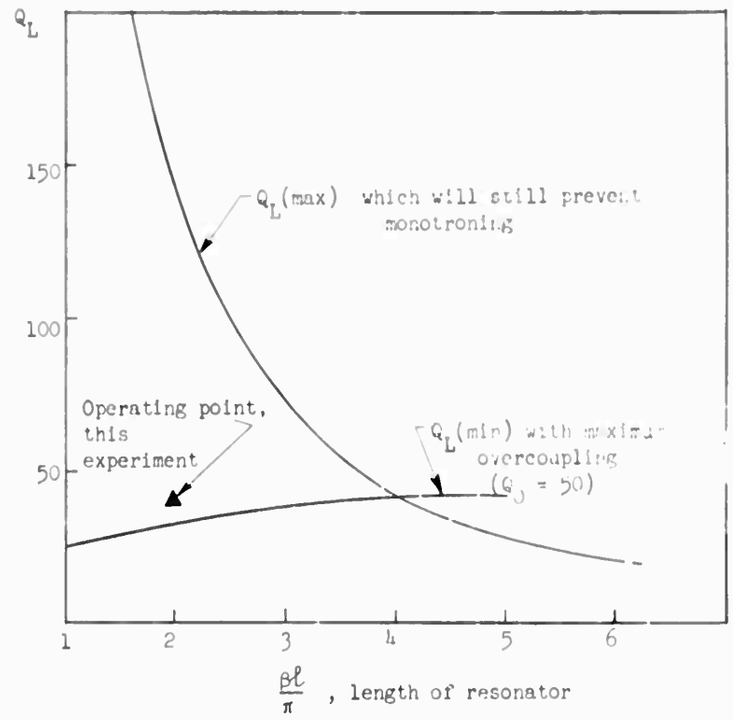

FIG. 5.4--Limits of operation for the output resonator

VI HOLLOW BEAM GUNS

A OBJECTIVE

The purpose of this project is to produce electron guns with high perveance and convergence. The most promising approaches to this problem are based on curvilinear flow instead of the more conventional rectilinear flows. For some time, the principal method of attack on the curvilinear flow problem has been through cut-and-try techniques. The goal here has been to reduce gun design for curvilinear flow to a more analytical and systematic scheme.

B. PRESENT STATUS

A promising way of designing hollow beam guns is through the use of the paraxial ray equation. With a view in mind of the practical application of this method, a method including magnetic field was developed during the year for determining the flow and the focusing electrodes to second order of axially symmetric systems. The method differs from work by others in the fact that the flow is found by solving ordinary differential equations instead of partial differential equations. This should insure greater speed, accuracy, and simplicity in the numerical calculations.

The basic approach used remains the same as with other work on the paraxial ray method. One chooses any two of these quantities along the central trajectory - voltage V , curvature K , and infinitesimal thickness, ξ . From this, the flow and focusing electrodes are calculated.

Our method depends on solving a set of simultaneous ordinary differential equations, known as the first-order, second-order, etc., paraxial ray equations. The solution of these equations yields quantities which can be used to find the edge trajectories, voltages and fields through a power series expansion about each point on the central trajectory.

Recalling that we are dealing with an axially symmetric system, we set a curvilinear coordinate system $(q_1 q_2 , \theta)$ A meridian section of this is shown in Fig. 6.1. The line $q_2 = 0$ is the central trajectory and $q_1 = 0$ is the cathode The magnetic field is assumed to lie tangential to the cathode, which implies that the vector potential, A , is zero along the cathode. The q_1 coordinate lines are assumed to be projections in the meridian plane of the trajectories We define s to be the arc length along the q_1-coordinate lines and ψ to be the angle of inclination of the q_1-coordinate lines. We also define h_1 and ξ as the rate of change of the arc length along the q_1- and q_2-coordinate lines with respect to q_1 and q_2 , respectively The variable h_1 is chosen to be unity along the central trajectory. Letting r and z be the usual cylindrical coordinates, we may then show from simple geometrical considerations that

$$\frac{\partial r}{\partial s} = \sin \psi \tag{6.1}$$

$$\frac{\partial z}{\partial s} = \cos \psi \tag{6.2}$$

$$\frac{\partial \psi}{\partial s} = K \tag{6.3}$$

$$\frac{\partial r}{\partial q_2} = \xi \cos \psi \tag{6.4}$$

$$\frac{\partial z}{\partial q_2} = - \xi \sin \psi \tag{6.5}$$

$$\frac{\partial \psi}{\partial q_2} = \frac{\partial \xi}{\partial s} \tag{6.6}$$

where $d/ds = (1/h_1)(\partial/\partial q_1)$.

As soon in Microwave Laboratory Report No 1037 (Quarterly Status Report No. 6 for this contract), we may write the voltage as

$$V = V_m + \frac{nA^2}{2} \tag{6.7}$$

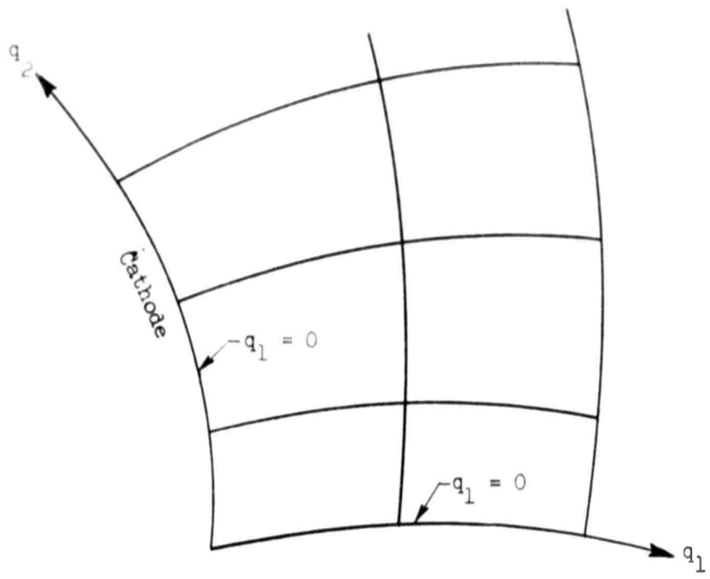

FIGURE 6.1

where V_m satisfies

$$\frac{\partial V_m}{\partial q_2} = 2\xi K V_m \quad . \tag{6.8}$$

The quantity V_m is a meridian voltage associated with the meridian velocity v_m, which is irrotational

$$\nabla \times v_m = 0 \tag{6.9}$$

By using Eq. (6.7) we may write Poisson's equation as

$$\nabla^2 V_m + \nabla^2 (nA^2/2) = \rho/\epsilon_0 \tag{6.10}$$

Upon expanding the first term in curvilinear coordinates and substituting for ρ, we obtain

$$\frac{1}{\xi r}\frac{d}{ds}\left(r\xi \frac{d}{ds} V_m\right) + \frac{\partial}{\partial q_2}\left(\frac{rh_1}{h_2}\frac{\partial V_m}{\partial q_2}\right) + \nabla^2\left(\frac{nA^2}{2}\right) \quad \frac{J_0 r_0 \xi_0}{\epsilon_0 v_m r h_2}, \tag{6.11}$$

where J_0, r_0, and ξ_0 are values at the cathode and $h_1 = ds/\partial q_1$. By expanding and simplifying, we obtain the first order paraxial ray equation:

$$2V_m\xi'' + \xi' V_m' + \xi(V_m'' + 4K^2 V_m) + \frac{\xi}{r}(V_m' \sin\psi + 2V_m K \cos\psi)$$

$$+ \eta\xi\left[B_r^2 + \left(B_z - \frac{A}{r}\right)^2 + \left(\frac{A}{r}\right)^2\right] = \frac{r_0 J_0 \xi_0}{\epsilon_0 r v_m} \quad , \tag{6.12}$$

where primes refer to derivatives with respect to s and where

$$V_m = V - \eta A^2/2 \tag{6.13}$$

$$V_m' = V - \eta A\left(\frac{\partial A}{\partial r}\sin\psi + \frac{\partial A}{\partial z}\cos\psi\right) \tag{6.14}$$

$$V_m'' = V'' - \eta\left(\frac{\partial A}{\partial r}\sin\psi + \frac{\partial A}{\partial r}\cos\psi\right)^2 - \eta A\left(\frac{\partial^2 A}{\partial r^2}\sin^2\psi + 2\frac{\partial^2 A}{\partial r\partial z}\sin\psi\cos\psi + \frac{\partial^2 A}{\partial z^2}\cos^2\psi\right) \tag{6.15}$$

In deriving the second-order paraxial ray equation, we use the two operator equations:

$$\frac{\partial}{\partial q_2}\frac{d}{ds} = \frac{d}{ds}\frac{\partial}{\partial q_2} + \xi K\frac{d}{ds} \tag{6.16}$$

$$\frac{\partial}{\partial q_2}\frac{d^2}{ds^2} = (\xi K)'\frac{d}{ds} + 2\xi K\frac{d^2}{ds^2} + \frac{d^2}{ds^2}\frac{\partial}{\partial q_2}\quad , \tag{6.17}$$

which are readily derived from the preceding equations. Differentiating Eq. (6.12) with $\partial/\partial q_2$ and applying Eqs. (6.16) and (6.17), we obtain

the second-order paraxial ray equation:

$$
\begin{aligned}
&- 5K\xi^2 V_m'' + \xi_q V_m'' + \xi_q' V_m' + 5\xi^2 K' V_m' + 2V_m \xi^2 K'' + 8V_m \xi K' \xi' + 4V_m K \xi'^2 \\
&+ 10 \frac{K\xi J_0 r_0 \xi_0}{r\, c_0 V_m} + 2V_m \xi_q'' + 4V_m K^2 \xi_q - 20\xi^2 K^3 V_m - \frac{J_0' r_0 \xi_0^2}{r\, c_0 V_m} \\
&+ \frac{\xi_q' V_m' \sin\psi}{r} - 6\frac{K\xi^2 V_m' \sin\psi}{r} + 2\frac{\xi^2 K' V_m \sin\psi}{r} - 2\frac{\xi^2 V_m' \sin\psi \cos\psi}{r^2} \\
&- 16\frac{\xi^2 V_m K^2 \cos\psi}{r} + 2\frac{KV_m \xi_q \cos\psi}{r} - 4\frac{KV_m \xi^2 \cos^2\psi}{r^2} - \frac{J_0 \xi_0^2 \cos\psi_0}{r\, c_0 V_m} \\
&+ 2\frac{J_0 r_0 \xi_0 \cos\psi\, \xi}{r^2 c_0 V_m} - \frac{\xi^2 V_m'' \cos\psi}{r} + \eta\xi_q \left[B_r^2 + \left(B_z - \frac{A}{r} \right)^2 + \left(\frac{A}{r} \right)^2 \right] \\
&+ 2\eta\xi^2 \left[B_r \left(\frac{\partial B_r}{\partial r} \cos\psi - \frac{\partial B_r}{\partial z} \sin\psi \right) + \left(B_z - \frac{A}{r} \right) \left(\frac{\partial B_z}{\partial r} \cos\psi \right. \right. \\
&\left. - \frac{\partial B_z}{\partial z} \sin\psi + \frac{A}{r^2} \cos\psi - \frac{1}{r} \frac{\partial A}{\partial r} \cos\psi + \frac{1}{r} \frac{\partial A}{\partial z} \sin\psi \right) \\
&\left. + \frac{A}{r^2} \left(\frac{\partial A}{\partial r} \cos\psi - \frac{\partial A}{\partial z} \sin\psi - \frac{A}{r} \cos\psi \right) \right] = 0 \quad , \qquad (6.18)
\end{aligned}
$$

where $\xi_q = \partial\xi/\partial q_2$.

Knowing, for example, V and K , Eqs. (6.1) - (6.3), (6.14) and (6.18) may be integrated simultaneously to obtain ξ and ξ_q .

These results can then be used to find the edge trajectory and voltages, as we shall now show

The quantities required at the beam edge for finding electrode shapes are $r^{(e)}$, $z^{(e)}$, $(\partial r/\partial q_1)^{(e)}$, $(\partial z/\partial q_1)^{(e)}$, $V^{(e)}$, and $V_n^{(e)} = (\partial V/h_2 dq_2)^{(e)}$, where superscript e refers to the beam edge. These may be expanded about the central trajectory in powers of dq_2 as follows:

$$r^{(e)} = r + \frac{\partial r}{\partial q_2} dq_2 + \frac{1}{2}\frac{\partial^2 r}{\partial q_2^2} dq_2^2 + \ldots \tag{6.19}$$

$$z^{(e)} = z + \frac{\partial z}{\partial q_2} dq_2 + \frac{1}{2}\frac{\partial^2 z}{\partial q_2^2} dq_2^2 + \ldots \tag{6.20}$$

$$\frac{\partial r^{(e)}}{\partial q_1} = \frac{\partial r}{\partial q_1} + \frac{\partial^2 r}{\partial q_1 \partial q_2} + \frac{1}{2}\frac{\partial^3 r}{\partial q_1 \partial q_2^2} + \ldots \tag{6.21}$$

$$\frac{\partial z^{(e)}}{\partial q_1} = \frac{\partial z}{\partial q_1} + \frac{\partial^2 z}{\partial q_1 \partial q_2} + \frac{1}{2}\frac{\partial^3 z}{\partial q_1 \partial q_2^2} + \ldots \tag{6.22}$$

$$V^{(e)} = V + \frac{\partial V}{\partial q_2} + \frac{1}{2}\frac{\partial^2 V}{\partial q_2^2} + \ldots \tag{6.23}$$

$$V_n^{(e)} = V_n + \frac{\partial V_n}{\partial q_2} + \frac{1}{2}\frac{\partial^2 V_n}{\partial q_2^2} + \ldots \tag{6.24}$$

The remaining problem is to find the coefficients on the right hand side

of these equations. The coefficients for Eqs. (6.19) - (6.22) are obtained solely from Eqs. (6.1) - (6.5) and (6.15) - (6.17).

$$\frac{\partial r}{\partial q_1} = \sin \psi \tag{6.25}$$

$$\frac{\partial z}{\partial q_1} = \cos \psi \tag{6.26}$$

$$\frac{\partial r}{\partial q_2} = \xi \cos \psi \tag{6.27}$$

$$\frac{\partial z}{\partial q_2} = - \xi \sin \psi \tag{6.28}$$

$$\frac{\partial^2 r}{\partial q_2^2} = \xi_q \cos \psi - \xi\xi' \sin \psi \tag{6.29}$$

$$\frac{\partial^2 z}{\partial q_2^2} = - \xi_q \sin \psi - \xi\xi' \cos \psi \tag{6.30}$$

$$\frac{\partial^2 r}{\partial q_1 \partial q_2} = \xi' \cos \psi - \xi K \sin \psi \tag{6.31}$$

$$\frac{\partial^2 z}{\partial q_1 \partial q_2} = - \xi' \sin \psi - \xi K \cos \psi \tag{6.32}$$

$$\frac{\partial^2 r}{\partial q_1 \partial q_2^2} = \cos \psi \left(\xi_q' - \xi\xi' K \right) - \sin \psi \left(K \xi_q + \xi\xi'' + \xi'^2 \right) \tag{6.33}$$

and

$$\frac{\partial^2 z}{\partial q_1 \partial q_2^2} = -\sin\psi\left(\xi_q' - \xi\xi' K\right) - \cos\psi\left(K\xi_q + \xi\xi'' + \xi'^2\right) \tag{6.34}$$

$$V_r = 2KV_m + \frac{\eta}{2}\left(\frac{\partial A^2}{\partial r}\cos\psi - \frac{\partial A^2}{\partial z}\sin\psi\right) \tag{6.35}$$

$$\frac{\partial V}{\partial q^2} = \xi V_n \tag{6.36}$$

$$\frac{\partial V_n}{\partial q_2} = 2V_m(\xi'' + 3K^2\xi) + \frac{\eta}{2}\left[\xi\left(\frac{\partial^2 A^2}{\partial r^2}\cos^2\psi - 2\frac{\partial^2 A^2}{\partial r\partial z}\sin\psi\cos\psi + \frac{\partial^2 A^2}{\partial z^2}\sin^2\psi\right) - \xi'\left(\frac{\partial A^2}{\partial r}\sin\psi + \frac{\partial A^2}{\partial z}\cos\psi\right)\right] \tag{6.37}$$

$$\frac{\partial^2 V}{\partial q_2^2} = \xi_q V_n + \xi\frac{\partial V_n}{\partial q_2} \tag{6.38}$$

$$\begin{aligned}\frac{\partial^2 V_n}{\partial q_2^2} = {} & 2V_m\left[3\xi_q K^2 + 12\xi^2 K^3 + 10K\xi\xi'' + \xi'^2 K + \xi K'\xi' + \xi_q''\right] \\ & + \frac{\eta}{2}\left\{\xi^2\left[\frac{\partial^3 A^2}{\partial r^3}\cos^3\psi - 3\frac{\partial^3 A^2}{\partial r^2\partial z}\cos^2\psi\sin\psi\right.\right. \\ & \left. + 3\frac{\partial^3 A^2}{\partial r\partial z^2}\sin^2\psi\cos\psi - \frac{\partial^3 A^2}{\partial z^3}\sin^3\psi\right] + \xi_q\left[\frac{\partial^2 A^2}{\partial r^2}\cos^2\psi\right. \\ & \left. - 2\frac{\partial^2 A^2}{\partial r\partial z}\sin\psi\cos\psi + \frac{\partial^2 A^2}{\partial z^2}\sin^2\psi\right] - 3\xi\xi'\left[\left(\frac{\partial^2 A^2}{\partial r^2} - \frac{\partial^2 A^2}{\partial z^2}\right)\sin\psi\cos\psi\right. \\ & \left. + \frac{\partial^2 A^2}{\partial r\partial z}\left(\cos^2\psi - \sin^2\psi\right)\right] \\ & - \left(\frac{\partial A^2}{\partial r}\sin\psi + \frac{\partial A^2}{\partial z}\cos\psi\right)\left(\xi_q' + \xi\xi' K\right) + \xi'^2\left(\frac{\partial A^2}{\partial z}\sin\psi - \frac{\partial A^2}{\partial r}\cos\psi\right)\Bigg\}.\end{aligned} \tag{6.39}$$

In summary, all the equations for the second-order approximation have been derived. Equations (6.1) - (6.3), (6.12), and (6.18) are first integrated. The results are then substituted into Eqs. (6.19) - (6.39) to determine the edge trajectories and coordinates. These in turn are integrated by analytic continuation methods to obtain the focusing electrodes.

VII. TRANSVERSE-WAVE STUDIES

A. TRANSVERSE-WAVE DEVICES

1. Introduction

The objective of this project is to study a possible approach to broadband high-powered amplifiers which involves interaction between an electron beam and a circuit in the presence of an axial dc magnetic field. This amplification mechanism depends on interaction between the transverse motion of the beam with transverse electric fields. Examples of such interaction are the Adler low-noise quadrupole amplifier, and the so-called fast-wave tubes where a rotating electron beam is interacting with an ordinary fast electromagnetic wave in a smooth waveguide. In the first case this type of interaction was used for low-noise amplifiers; in the second case, for very high frequency amplifiers. There are many possible variations of this kind of interaction, however, which would be appropriate to any frequency range and not merely for low noise.

2. Background

The theoretical work on transverse-wave propagation done during the last year has led to a better understanding of transverse waves. In particular, the work has led to improvements in the filamentary beam theory for ordinary cyclotron and synchronous waves. In addition, the work has pointed out the existence of other transverse-wave types with properties that are entirely different from the ordinary transverse waves. These new waves can exist on beams having rotational motion. The required power for interaction with external circuits is supplied by the rotational dc energy of the beam. In this sense these waves are different from the ordinary transverse waves and longitudinal space-charge waves which take their energy from the longitudinal drift motion.

Some of the properties of the new transverse waves are very interesting, in the sense that they lead to possible interaction schemes which overcome some of the shortcomings suffered by ordinary transverse-wave devices, in particular, with respect to efficiency and simplicity of the circuits. This is due to the fact that some of the new waves combine the unusual properties of being fast waves with infinite or nearly infinite phase velocity, and also alternately the carriers of negative energy.

Due to these relatively recent results the emphasis has been shifted from ordinary transverse interaction towards the investigation of the new transverse waves which we shall refer to as force-free waves. The name comes from the fact that in a field analysis these waves are characterized by zero electric field inside the beam.

We shall present a simplified theory for the occurrence of the force-free waves based on an approach which involves only the equation of continuity and the force equation. We shall neglect external fields due to space-charge (which are zero or very small in the force-free waves).

3 Theory of Bunching in Transverse-Wave Devices

Let us assume a simple balanced beam model in which the individual electrons are rotating around the axis with the cyclotron frequency ω_c. Such a beam can, for instance, be established by a magnetic field reversal. The dc beam is characterized by

$$\vec{v}_0 = \omega_c r \vec{a}_\phi + v_0 \vec{a}_z \tag{7.1}$$

$$\rho_0 = \text{constant} \quad .$$

The equation of continuity is

$$\nabla \cdot \vec{I} + j\omega\rho = 0 \quad . \tag{7.2}$$

The definition of current is

$$\vec{I} = \rho_0 \vec{v} + \rho \vec{v}_0 \quad . \tag{7.3}$$

Hence,

$$\nabla \cdot \vec{i} = \rho_0 \nabla \cdot \vec{v} - jm\omega_c \rho + v_0 \frac{d\rho}{dz} \quad , \tag{7.4}$$

where we have assumed the wave in consideration to vary as $\exp(-j\phi)$. Substitution in (7.2) yields

$$\left(j \frac{\omega - \omega_c}{v_0} + \frac{d}{dz} \right) \rho = - \frac{\rho_0}{v_0} \nabla \cdot \vec{v} \quad . \tag{7.5}$$

Let

$$\frac{\omega - \omega_c}{v_0} = \beta_e - \beta_c = \beta_1 \quad . \tag{7.6}$$

Then, the solution of (7.5) is

$$\rho = \frac{\rho_0}{v_0} e^{-j\beta_1 z} \int_0^z (\nabla \cdot \vec{v}) \, e^{j\beta_1 z} \, dz \quad . \tag{7.7}$$

This relation gives the rf charge density in terms of the divergence of the rf velocity $\vec{v}$. Equation (7.7) shows that the space-charge density essentially is a periodic function in z with periodicity determined by the propagation factor $\beta_1 = \beta_e - \beta_c$. The amount of bunching that takes place is determined by the divergence of the velocity $\vec{v}$. For waves characterized by $\exp(-j\phi)$ variation we obtain

$$\nabla \cdot \vec{v} = \frac{1}{2} \frac{\partial v_+}{\partial r} + \frac{v_-}{r} + \frac{1}{2} \frac{\partial v_-}{\partial r} + \frac{\partial v_z}{\partial z} \quad . \tag{7.8}$$

The velocity components can be determined from the force equations which for the present case are:

$$\left[J\beta_{+} + \frac{d}{dz}\right] v_{+} = -\frac{\eta}{v_0}\left[E_{+} + Jv_0 B_{+} + \omega_c r B_z\right] \tag{7.9}$$

$$\left[J(\beta_{-} - \beta_c) + \frac{d}{dz}\right] v_{-} = -\frac{\eta}{v_0}\left[E_{-} - Jv_0 B_{-} + \omega_c r B_z\right] \tag{7.10}$$

$$\left[J(\beta_{-} - \beta_c) + \frac{d}{dz}\right] v_z = -\frac{\eta}{v_0}\left[E_z - \omega r \frac{B_{+} + B_{-}}{2}\right] \tag{7.11}$$

where

$$\begin{aligned} v_{+} &= v_r + Jv_\phi \\ v_{-} &= v_r - Jv_\phi \end{aligned} \tag{7.12}$$

and similarly for the field components.

We shall use the paraxial expressions for the components of the circuit field. For the mode varying as $\exp(-J\phi)$, the paraxial components are

$$\begin{cases} E_{-} = 0 \\ B_{-} = 0 \end{cases} \tag{7.13}$$

$$\begin{cases} E_{+} \text{ is independent of } r \\ B_{+} \text{ is independent of } r \end{cases} \tag{7.14}$$

$$E_z = \frac{1}{2}\left[\frac{d}{dz} E_{+} + \omega B_{+}\right] r = \hat{E}_z r \tag{7.15}$$

$$B_z = \frac{1}{2}\left[\frac{d}{dz} B_{+} - \frac{\omega}{c^2} E_{+}\right] r = \hat{B}_z r \quad . \tag{7.16}$$

By solving for the velocity components, we obtain

$$v_+ = \frac{\eta}{v_0} e^{-j\beta_e z} \int_0^z \left[E_+ + jv_0 B_+ + \omega_c r^2 \hat{B}_z \right] e^{j\beta_e x} \, dx \qquad (7.17)$$

$$v_- = -\frac{\eta}{v_0} \omega_c r^2 e^{-j(\beta_e - 2\beta_c)z} \int_0^z \hat{B}_z \, e^{j(\beta_e - 2\beta_c)x} \, dx \qquad (7.18)$$

$$v_z = -\frac{\eta}{v_0} e^{-j(\beta_e - \beta_c)z} r \int_0^z \left[\hat{E}_z - \frac{\omega_c}{2} B_+ \right] e^{j(\beta_e - \beta_c)x} \, dx \; . \qquad (7.19)$$

The paraxial field components appearing in the equations are functions of z, but not of r. It is now a simple matter to calculate $\nabla \cdot \vec{v}$ from (7.8). We obtain

$$\nabla \cdot \vec{v} = -\frac{\eta}{v_0} \omega_c r \left\{ e^{-j\beta_e z} \int_0^z \hat{B}_z \, e^{j\beta_e x} \, dx + 2e^{-j(\beta_e - 2\beta_c)z} \int_0^z \hat{B}_z \, e^{j(\beta_e - 2\beta_c)x} \, dx \right.$$

$$\left. + \frac{d}{dz} \left[e^{-j(\beta_e - \beta_c)z} \int_0^z \left(\frac{\hat{E}_z}{\omega_c} - \frac{1}{2} B_+ \right) e^{j(\beta_e - \beta_c)x} \, dx \right] \right\} \; . \qquad (7.20)$$

Since the bunching is determined by $\nabla \cdot \vec{v}$, we can draw a number of important conclusions from Eq. (7.20).

These conclusions pertain to a circuit field characterized by $\exp(-j\phi)$ variation and a beam with rotational frequency ω_c:

a. The <u>transverse electric field</u> E_+ does not contribute to bunching. Physically, this is tied in with the fact that the rotational frequency ω_c is independent of radial position. The transit time for one revolution is independent of radius.

b. The axial magnetic field $\hat{B}_z$ produces some bunching which arises from transverse velocity modulation proportional to r^2. This velocity modulation depends on the radius and therefore contributes to $\dot{r} \cdot \dot{V}$, and therefore to ρ.

c. The transverse magnetic field B_+ and the longitudinal electric field E_z contribute to bunching due to longitudinal velocity modulation.

The relative contributions from the field components B_z, B_+ and E_z can be determined by calculating the integral in Eq. (7.7). Results follow from Eq. (7.10). For convenience, we like to separate the various contributions, writing

$$\frac{\rho}{\rho_0} = \frac{1}{\rho_0}\rho_{B_z} + \frac{1}{\rho_0}\rho_{B_+} + \frac{1}{\rho_0}\rho_{E_z} \quad . \tag{7.21}$$

We obtain

$$\frac{1}{\rho_0}\rho_{B_z} = \frac{1}{2} J \frac{v_0}{V_0} r \int_0^z \hat{B}_z e^{-J\beta_1(z-x)} dx \tag{7.22}$$

$$\frac{1}{\rho_0}\rho_{B_+} = -\frac{1}{4V_0}\omega_c r \left[1 + \beta_1 \frac{d}{d\beta_1}\right] \int_0^z B_+ e^{-J\beta_1(z-x)} dx \tag{7.23}$$

$$\frac{1}{\rho_0}\rho_{E_z} = \frac{1}{2V_0} r \left[1 + \beta_1 \frac{d}{d\beta_1}\right] \int_0^z \hat{E}_z e^{-J\beta_1(z-x)} dx \quad , \tag{7.24}$$

where

$$\beta_1 = \beta_e - \beta_c \tag{7.25}$$

$$V_0 = \frac{1}{2}\frac{v_0^2}{\eta} \quad . \tag{7.26}$$

By using the paraxial expressions (7.15) and (7.16) we can express the equations in terms of the transverse field components only. We obtain

$$\frac{1}{\rho_0}\rho_{B_z} = \frac{1}{4} j \frac{v_0}{V_0} r \left\{ B_+(z) - j\beta_1 \int_0^z B_+ e^{-j\beta_1(z-x)}\, dx - \frac{\omega}{c^2} \int_0^z E_+ e^{-j\beta_1(z-x)}\, dx \right\} \tag{7.27}$$

$$\frac{1}{\rho_0}\rho_{B_+} = -\frac{1}{4V_0}\omega_c r \left[1 + \beta_1 \frac{d}{d\beta_1}\right] \int_0^z B_+ e^{-j\beta_1(z-x)}\, dx \tag{7.28}$$

$$\frac{1}{\rho_0}\rho_{E_z} = \frac{1}{4V_0} r \left[1 + \beta_1 \frac{d}{d\beta_1}\right] \left\{ E_+(z) - j\beta_1 \int_0^z E_+ e^{-j\beta_1(z-x)}\, dx + \omega \int_0^z B_+ e^{-j\beta_1(z-x)}\, dx \right\} . \tag{7.29}$$

These paraxial equations hold for any circuit field, and they automatically account for the rf stray fields at the ends of the circuit, i.e., end effects are taken into account. These end effects can be quite important for bunching in certain special cases. For instance, if the circuit is a TE mode in a waveguide operated at or near cutoff, the transverse magnetic field B_+ is negligible, and the main contribution to bunching is from the axial electric stray field E_z at the input end of the circuit.

Once the rf bunching is established the corresponding rf currents are

$$i_+ \approx \rho\, \omega_c r \tag{7.30}$$

$$i_z \approx \rho\, v_0 \quad . \tag{7.31}$$

In a fast-wave device most of the dc kinetic energy is rotational. Hence i_+ is considerably larger than i_z, and will interact strongly with the transverse electric field. If the relative phase between current and field

is correct, energy is extracted from the beam, and the interaction principle can be used to obtain oscillations.

4. Experimental Work

The principle outlined above has been used in an experimental oscillator consisting of a simple Cuccia coupler and a hollow beam rotating at the cyclotron frequency. The oscillator has been tested and some small output power observed. The details are described in a technical report.[1]

B. SPACE-CHARGE WAVES IN AN ACCELERATED PARALLEL-FLOW ELECTRON BEAM IN A CONSTANT MAGNETIC FIELD

1. Statement of the Problem

Consider a parallel-flow Pierce electron gun as shown in Fig. 7 1. For this type of gun the electrodes are shaped in such a way that the unperturbed electric forces acting on the electrons are in the axial (z-) direction only. The equations describing the drift velocity $(\vec{v}_0)$ are therefore essentially those of a space-charge limited diode. In addition to the axial electric field $(\vec{E}_0)$, there is also an applied dc magnetic field $(\vec{B}_{0z})$.

The problem is concerned with finding the small perturbed velocity and field quantities at plane (b) in terms of these quantities at plane (a). Plane (a) is assumed to lie just beyond the potential minimum of the beam and the initial velocity and charge disturbance at this plane are quite arbitrary.

By assuming that the perturbations are taken small enough, Maxwell's equations can be appropriately linearized. Furthermore, the velocity at any point is assumed to be single-valued, and no electron collisions are supposed to occur.

2. Scope of the Research

It is the scope of this research to establish the general transformation properties in accelerated regions, involving not only the fundamental space-charge mode but also θ-varying modes (transverse waves). These problems

---

[1] T. Wessel-Berg and R. Hayes, "A New Transverse-wave Monotron Oscillator," Microwave Laboratory Report No. 1070, Stanford University (July 1963).

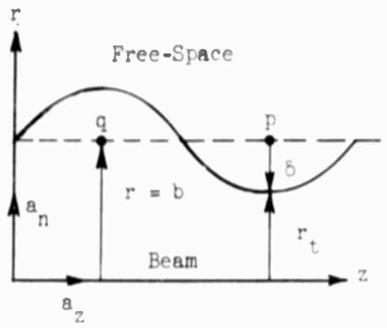

FIGURE 7.2

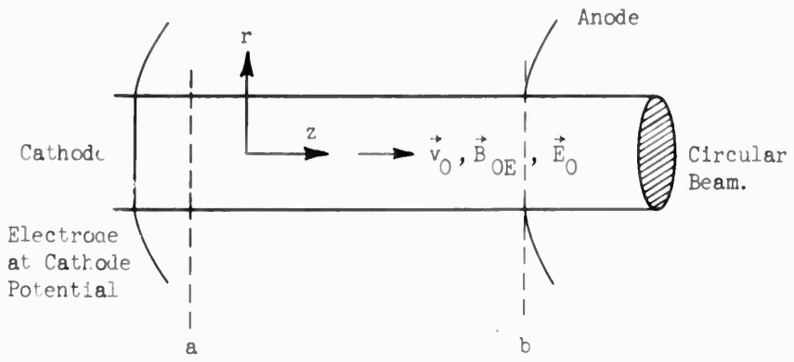

FIG. 7.1--Pierce electron gun.

are of basic importance for the understanding and theory of noise reduction schemes in linear beam amplifiers. In particular, it is hoped that the inclusion of space-varying modes will lead to better understanding of the noise properties of transverse wave amplifiers such as cyclotron wave devices.

Smullin[1] and Müller[2] have considered an accelerated electron beam in which the transverse velocity and field components are absent and in which the longitudinal components depend upon the axial coordinate only. In particular, Müller has shown that the longitudinal velocity noise components are in general attenuated on an accelerated electron beam and amplified on a decelerated beam. In view of this, it is anticipated that approximately the same results hold for the longitudinal noise components when the beam is subjected to a three-dimensional analysis in the cylindrical coordinates (r, θ, z). With regard to the transverse noise components, however, no conclusions can be drawn from the quoted papers, especially when an applied constant magnetic field is present.

b. The Beam Equations

The three-dimensional beam equations consist of seven independent Maxwell's equations and the three independent force equations, namely (in MKS units):

$$\nabla \times \vec{E}_t + \frac{\partial \vec{B}_t}{\partial t} = 0 \tag{7.32}$$

$$\nabla \times \vec{B}_t - \frac{1}{c^2} \frac{\partial \vec{E}_t}{\partial t} = \mu_0 \rho_t \vec{v}_t \tag{7.33}$$

$$\nabla \cdot \vec{E}_t = \rho_t / \epsilon_0 \tag{7.34}$$

$$\frac{d}{dt}\left(\vec{v}_t / \sqrt{1 - \frac{1}{c^2} |\vec{v}_t|^2} \right) = \frac{e}{m_0} (\vec{E}_t + \vec{v}_t \times \vec{B}_t) \tag{7.35}$$

---

(1) L. D. Smullin, "Propagation of Disturbances in One-dimensional Electron Streams," J. Appl. Phys. 22, 1496-8 (December 1951).

(2) R. Müller, "Raumladungswellen in beschleunigten und versögerten eindimensionalen Elektronenströmungen," Arch. fur Elektrische Übertragung 9, 505-12 (August 1955).

where the subscript (t) denotes a total quantity and

$e(<0)$ = electron charge,

m_0 = electron rest mass,

ϵ_0 = inductive capacity in vacuum,

μ_0 = permeability in vacuum,

$c = 1/\sqrt{\mu_0 \epsilon_0}$ = speed of light,

t = time,

ρ_t = charge density,

$\vec{v}_t$ = velocity,

$\vec{E}_t$ = electric field intensity, and

$\vec{B}_t$ = magnetic flux density .

In order to made an analytic solution of the system (7.32) - (7.35) feasible, the following simplifying assumptions will be made.

(a) In view of the geometry in Fig. 7.1, a circular cylindrical coordinate system (r , θ , z) will be used. Hence,

$$\nabla = \vec{a}_r \frac{\partial}{\partial r} + \vec{a}_\theta \frac{1}{r} \frac{\partial}{\partial \theta} + \vec{a}_z \frac{\partial}{\partial z} \quad .$$

(b) The small-signal analysis together with the Eulerian[1] description of (7.35) is applied. If (ϕ_0) and (ϕ) are dc and ac functions, respectively, then the solutions will generally be of the form:

$$\phi_t(r , \theta , z , t) = \phi_0(z) + \phi (r , \theta , z , t) . \; ; \; |\phi| \ll |\phi_0| \quad .$$

Thus products of two or more ac terms will be neglected so that the beam equations become linear.

(c) Apart from the fact that dc electron flow can not remain parallel at relativistic speeds in the usual Pierce gun design (due to the pinching effect of the tangential magnetic field created by the beam current), the

---

[1] D. L. Bobroff, "Independent Space Variables for Small-Signal Electron Beam Analyses," IRE, Trans. PGED, 68 (January 1959).

complications arising from a relativistic treatment are too great. We have shown elsewhere that no coordinate transformation exists (such as the Lorentz transformation, in the case where the drift velocity is constant), which simplifies the beam equations. Thus the relativistic term in (7.3) will henceforth be dropped, and the parallel flow conditions inside the beam are given by

$$\vec{E}_0 = \hat{a}_z E_0(z) \; ; \; \vec{v}_0 = \hat{a}_z v_0(z) \; ; \; |v_0| < c \qquad (7.36)$$

(c) The total dc magnetic field ($\vec{B}_0$) consists of a constant axial applied field (B_{0z}) in the axial direction and a radially-varying azimuthal field ($B_{0\theta}$) due to the beam current. Since the effect of ($B_{0\theta}$) upon the transverse noise signal is of main interest in the present analysis, the field ($B_{0\theta}$) will be neglected in the beam equations. Thus inside the beam

$$\vec{B}_0 = \hat{a}_\theta B_{0\theta}(r) + \hat{a}_z B_{0z} \; ; \; |B_{0\theta}| \ll |B_{0z}| \qquad (7.37)$$

In view of the above considerations, Eqs. (7.32) - (7.35) become

dc part:

$$\nabla \times \vec{E}_0 = 0 \; ; \; \nabla \times \vec{B}_0 = \mu_0 \rho_0 \vec{v}_0 \; ; \; \nabla \cdot \vec{E}_0 = \rho_0/\varepsilon_0 \; , \; \vec{v}_0 \cdot \nabla \vec{E}_0 \qquad (7.38)$$

ac part:

$$\nabla \times \vec{E} + \frac{\partial \vec{B}}{\partial t} = 0 \qquad (7.39)$$

$$\nabla \times \vec{B} - \frac{1}{c^2} \frac{\partial \vec{E}}{\partial t} = \mu_0 (\rho_0 \vec{v} + \rho \vec{v}_0) \qquad (7.40)$$

$$\nabla \cdot \vec{E} = \rho/\varepsilon_0 \qquad (7.41)$$

$$\left(\frac{\partial}{\partial t} + \vec{v}_0 \cdot \nabla \right) (p\vec{v}) + \vec{v}_0 \nabla (q\vec{v}_0) = \eta (\vec{E} + \vec{v} \times \vec{B}_{0z} + \vec{v}_0 \times \vec{B}) \; , \qquad (7.42)$$

where $\eta = e/m^0$, and $p = q = 1$.

The solutions of the system (7.39) - (7.42) are subject to:

(a) The dc solutions of (7.38).

(b) The boundary conditions at the beam radius (b) .

(c) The solutions of the ac free-space equations outside the beam. These equations follow at once from Eqs. (7.39) and (7.40), namely,

$$\nabla \times \vec{E} + \frac{\partial \vec{B}}{\partial t} = 0 \qquad (7.43)$$

$$\nabla \times \vec{B} - \frac{1}{c^2} \frac{\partial \vec{E}}{\partial t} = 0 \qquad (7.44)$$

(d) The boundary conditions at infinite radius (r) . It is assumed that all free-space fields vanish at this radius.

(e) The initial conditions at plane (a) in Fig. 7.1.

After the system (7.39) - (7.42) has been integrated with respect to (r , θ , t) , there results an eighth-order differential system with the variable coefficients $\rho_0(z)$ and $v_0(z)$. We will show that if ρ_0 and v_0 are constant (ion-neutralized beam), a Lorentz transformation reduces the order of this system by four. It however appears that when (ρ_0) and (v_0) are functions of (z) no such simplifying transformations exist. We have found that in order to arrive at a practical solution of this system, one has to impose quasi-static approximations (reducing the system to the sixth-order) and solve this system by means of the WKB method.[1] Other methods, such as variational methods, are still being investigated. Although ranges of validity for the WKB method have been known for some time in view of the solution of Schrödinger's equation (second-order), only recently Shkarofsky[2] has considered its validity for higher-order systems (fourth-order). Apart from the validity of the WKB method one also has to consider the ranges of validity of the quasi-static approximations. Although Rigrod[3] has indicated some of the

---

[1] J. Heading, An Introduction to Phase-Integral Methods, New York, John Wiley (1962).

[2] I. P. Shkarofsky, "Longitudinal Waves in an Inhomogeneous Magnetic Field-Plasma Interface Based on the WKB Approximation," Canadian J. of Phys. 41, 569-80 (April 1963).

[3] W. W. Rigrod, "Space-Charge Waves Along Magnetically-Focused Electron Beams," Proc. IRE 46, 358-9 (January 1958).

conditions to be imposed on this type of approximation, we do not believe them to be generally valid. In order to obtain more precise definitions in this respect we shall therefore also consider Hahn's[1] model of an ion-neutralized beam. Since in this model (ρ_0) and (v_0) are constant, the beam equations can be readily integrated with respect to (z). It turns out that when the relativistic term is included in the force equations, the beam determinantal equation becomes simpler. Provided the ion mass is very large compared to the electron mass, Eqs. (7.39) - (7.42) together with $p = (1 - v_0^2/c^2)^{-\frac{1}{2}}$ and $q = 0$ apply equally well to this problem.

After starting out with the relativistic beam, boundary and free-space determinantal equations which take θ-dependency into account (Hahn did not consider this) we will then briefly consider some elementary solutions for the quasi-static and thin-beam case.

4. DC Solutions

(a) Space-Charge Limited Beam

Putting in Eqs. (7.38),

$$\vec{E}_0 = -\nabla \phi_0 \equiv -\vec{a}_z \frac{\partial \phi_0}{\partial z} \quad ,$$

one obtains, after making substitutions and performing a first integration, the differential equation which must be satisfied by the dc potential (ϕ_0), namely

$$\left(\frac{d\phi_0}{dz}\right)^2 = -\frac{4I_0}{\epsilon_0}(-2\eta)^{-\frac{1}{2}}(\phi_0^{\frac{1}{2}} + A_1) \quad , \qquad (7.45)$$

where $\vec{I}_0 = \rho_0(z)\,\vec{v}_0(z)$ is the constant dc beam current beyond the potential minimum $(z = 0)$ away from the cathode and (A_1) is a constant of integration. Imposing the conditions $\phi_0 = E_0 = v_0 = 0$ at $z = 0$, so that from (7.45) $A_1 = 0$, the well-known Child's relations for a space-charge limited parallel plane diode are obtained. In terms of both (z) and the

---

[1] W. C. Hahn, "Small Signal Theory of Velocity-modulated Electron Beams," G. E. Rev. 42, 258-70 (June 1939).

dc electron transit time (τ) these are:

$$\left\{\begin{aligned} v_0 &= \frac{dz}{d\tau} = 3\left(\frac{\eta I_0}{6\epsilon_0}\right)^{1/3} z^{2/3} = \left(\frac{\eta I_0}{2\epsilon_0}\right)\tau^2 \; ; \; \rho_0 = \frac{I_0}{v_0} \\ z &= \left(\frac{\eta I_0}{6\epsilon_0}\right)\tau^3 \\ E_0 &= \left(\frac{6}{\eta}\right)\left(\frac{\eta I_0}{6\epsilon_0}\right)^{2/3} z^{1/3} = \frac{I_0}{\epsilon_0}\tau \\ \phi_0 &= -\left(\frac{9}{2\eta}\right)\left(\frac{\eta I_0}{6\epsilon_0}\right)^{2/3} z^{4/3} = -\left(\frac{\eta I_0^2}{8\epsilon_0^2}\right)\tau^4 \quad . \end{aligned}\right. \tag{7.46}$$

The tangential magnetic field $(B_{0\theta})$ due to the beam current (I_0) is found by performing simple line and surface integration in a plane of constant (z) in the expression:

$$\oint \vec{B}_0 \cdot \vec{d\ell} = \mu_0 \int \vec{I}_0 \cdot \vec{ds} \quad .$$

If (b) is the beam radius, then

$$\left.\begin{aligned} B_{0\theta}^{-} &= \tfrac{1}{2}\mu_0 I_0 r \quad , \quad r < b \\ B_{0\theta}^{+} &= \tfrac{1}{2}\mu_0 I_0 b^2/r \quad , \quad r > b \end{aligned}\right\} \quad . \tag{7.47}$$

(b) Ion-Neutralized Beam

In Hahn's beam model, which we will consider here, the electron beam is supposed to be well-mixed with an ion beam. For these two beams, space-charge densities are equal in magnitude and of opposite polarity, dc flow speeds and directions are the same and the average beam radii are

likewise equal. The dc velocities as well as the space-charge densities are constant and no tangential dc magnetic field is present since the net dc beam current is zero. Consequently, relativistic parallel flow is possible in this case.

5. Boundary Conditions

(a) Space-Charge Limited Beam

It has been shown by White[1] and others that the rippled beam edge in Fig. 7.2 can be replaced by a straight beam edge on which an equivalent surface current density $(\vec{S})$ and surface charge density (σ) exists. The boundary conditions are given by

$$\vec{a}_r \cdot (\vec{B}^+ - \vec{B}^-) = 0 \quad ; \quad \vec{a}_r \times (\vec{B}^+ - \vec{B}^-) = \mu_0 \vec{S}$$
$$\vec{a}_r \times (\vec{E}^+ - \vec{E}^-) = 0 \quad ; \quad \vec{a}_r \cdot (\vec{E}^+ - \vec{E}^-) = \sigma/\epsilon_0 \quad , \tag{7.48}$$

where the superscript $(+)$ refers to the ac fields outside the beam evaluated at an average radius (b). The quantities $(\vec{S})$ and (σ) can be expressed in terms of the beam ripple (δ) as follows. Let (ϕ) in this case represent either the electric ac potential or any of the ac components of $(\vec{B})$ and $(\vec{E})$. Then if the total radius (r_t) is defined by

$$r_t(r, \theta, z, t) = r + \delta(r, \theta, z, t) \quad ; \quad |\delta| \ll |r| = b \quad , \tag{7.49}$$

a first-order Taylor expansion of the total potential (ϕ_t) about the average radius $(r = b)$ yields (in the case of axial symmetry):

$$\phi_t(r_t, \theta, z, t) = \phi_0[(r + \delta), z] + \phi[(r + \delta), \theta, z, t]$$
$$\approx \phi_0(b, z) + \phi(b, \theta, z, t) + \left.\frac{\partial \phi_0}{\partial r}\right|_b \delta(b, \theta, z, t) \quad , \tag{7.50}$$

since $|\phi_0| \gg |\phi|$.

---

[1] G. R. White, "Space-Charge Waves in Relativistic Brillouin Beams," Proc. Int. Cong. on Microwave Tubes, Munich, June 1960, pp. 271-3, New York, Academic Press (1961).

Equating the total inside and outside potentials at the rippled beam edge (r_t), Eq. (20) yields

$$\phi_0^+(b,z) - \phi_0^-(b,z) = 0 \tag{7.51}$$

$$\phi^+(b,\theta,z,t) - \phi^-(b,\theta,z,t) = \left(- \left.\frac{\partial \phi_0^+}{\partial r}\right|_b + \left.\frac{\partial \phi_0^-}{\partial r}\right|_b \right) \delta(b,\theta,z,t) \quad . \tag{7.52}$$

Replacing (ϕ) in (7.51) and (7.52) by $(\vec{B})$ and $(\vec{E})$, respectively, one obtains from (7.48):

$$\vec{B}_0^+(b,z) = \vec{B}_0^-(b,z) \quad ; \quad \vec{E}_0^+(b,z) = \vec{E}_0^-(b,z) \tag{7.53}$$

$$\vec{S} = \frac{1}{\mu_0} \vec{a}_r \times \left(- \left.\frac{\partial \vec{E}_0^+}{\partial r}\right|_b + \left.\frac{\partial \vec{B}_0^-}{\partial r}\right|_b \right) \delta(b,\theta,z,t) \tag{7.54}$$

$$\sigma = \epsilon_0 \vec{a}_r \cdot \left(- \left.\frac{\partial \vec{E}_0^+}{\partial r}\right|_b + \left.\frac{\partial \vec{E}_0^-}{\partial r}\right|_b \right) \delta(b,\theta,z,t) \quad . \tag{7.55}$$

Since (B_{0z}) is constant and $(B_{0\theta})$ is given by (7.47) it follows from (7.54) that:

$$\vec{S} = \vec{a}_z \, I_0 \, \delta(b,\theta,z,t) \quad ; \quad I_0 = \rho_0(z) \, v_0(z) = \text{const.} \tag{7.56}$$

Making use of (7.53) and the relations

$$\nabla \cdot \vec{E}_0^+ = \vec{a}_r \cdot \frac{\partial \vec{E}_0^+}{\partial r} + \vec{a}_z \cdot \frac{\partial \vec{E}_0^+}{\partial z} = 0 \quad ,$$

$$\nabla \cdot \vec{E}_0^- = \vec{a}_z \cdot \frac{\partial \vec{E}_0^-}{\partial z} = \rho_0(z)/\epsilon_0 \quad ,$$

it is then easily verified that (7.55) becomes:

$$\sigma = \rho_0(z) \, \delta(b,\theta,z,t) \quad . \tag{7.57}$$

(b) Ion-Neutralized Beam

Referring to Fig. 7.2, Hahn assumes in his beam model that all ions and electrons are contained within the perturbed beam boundary. The ion space-charge density is constant everywhere and the total electron current through any plane of constant (z) is conserved. Hence with the aid of (7.49) we have at radius (b) to the first-order for the current per unit area,

$$S_z = -\frac{1}{2\pi b \mu_0} \oint \vec{B} \cdot d\vec{\ell} \approx -B_\theta/\mu_0 \qquad (7.58)$$

$$= -\left(\frac{1}{2\pi b}\right) \pi \rho_0 v_0 (b^2 - r_t^2) \approx I_0 \delta(b,\theta,z,t) \ ,$$

and for the charge per unit area,

$$\sigma = -\frac{\epsilon_0}{2\pi b} \int \vec{E} \cdot d\vec{s} = -\epsilon_0 E_r \qquad (7.59)$$

$$= -\left(\frac{1}{2\pi b}\right) \pi \rho_0 (b^2 - r_t^2) \approx \rho_0 \delta(b,\theta,z,t) \ .$$

Since (B_θ , E_r) are fields just outside the boundary, they must be added to the free-space fields (B_θ^+ , E_r^+) , respectively. In view of (7.58) and (7.59) it can then be shown that the boundary conditions

$$B_\theta^+ + B_\theta = B_\theta^- \ ; \ E_r^+ + E_r = E_r^-$$

are identical with those of the space-charge limited parallel flow as discussed previously.

(c) Dependency of the Boundary Conditions

By subtracting the radial parts of Maxwell's beam equations (7.39), (7.40) from those in free space (7.43), (7.44), the dependency of the

boundary conditions (7.48) upon each other is easily seen from:

$$\nabla \cdot [\vec{a}_r \times (\vec{E}^+ - \vec{E}^-)] - \frac{\partial}{\partial t} [\vec{a}_r \cdot (\vec{B}^+ - \vec{B}^-)] = 0 \qquad (7.60)$$

$$\nabla \cdot [\vec{a}_r \times (\vec{B}^+ - \vec{B}^-)] + \frac{1}{c^2} \frac{\partial}{\partial t} [\vec{a}_r \cdot (\vec{E}^+ - \vec{E}^-)] = \mu_0 \rho_0 v_r (b,\theta,z,t) \quad . \qquad (7.61)$$

If further in view of (7.48) Eqs. (7.56) and (7.57) are substituted into (7.61), one obtains

$$v_r(b,\theta,z,t) = \left(\frac{\partial}{\partial t} + v_0 \frac{\partial}{\partial z}\right) \delta(b,\theta,z,t) \equiv \frac{d\delta}{dt} \quad , \qquad (7.62)$$

which in fact is the Eulerian derivative of (δ) as it should be. Hence of the three boundary conditions which are contained in either (7.60) or (7.61), at least two must be specified. This brings the total number of independent boundary conditions to four.

After elimination of (δ), our independent boundary conditions are then given by

$$\begin{cases} E_\theta^+ - E_\theta^- = E_z^+ - E_z^- = 0 \; ; \; B_z^+ - B_z^- = 0 \; ; \\ B_\theta^+ - B_\theta^- = \dfrac{v_0(z)}{c^2} (E_r^+ - E_r^-) \quad . \end{cases} \qquad (7.63)$$

As has been pointed out before, (7.63) applies to either the space-charge limited case or the ion-neutralized case $(v_0 = \text{const.})$.

6. AC Solutions

In view of the remarks in Sec. 3, we proceed briefly as follows. Substituting into Eqs. (7.39) - (7.42) the elementary solutions:

$$\begin{cases} E_r = [-J_m'(\gamma r)\, \hat{E}_r(z) + \frac{jm}{\gamma r} J_m(\gamma r)\, \hat{E}_\theta(z)]\, e^{j(\omega t + m\theta)} \\ E_\theta = [-J_m'(\gamma r)\, \hat{E}_\theta(z) - \frac{jm}{\gamma r} J_m(\gamma r)\, \hat{E}_r(z)]\, e^{j(\omega t + m\theta)} \\ E_z = J_m(\gamma r)\, \hat{E}_z(z)\, e^{j(\omega t + m\theta)} \\ \rho = J_m(\gamma r)\, \hat{\rho}(z)\, e^{j(\omega t + m\theta)} \quad , \end{cases} \qquad (7.64)$$

and similar solutions for all other vectors and scalars, one obtains the eighth-order system:

$$\frac{d\hat{E}_r}{dz} = -\gamma \hat{E}_z - j\omega \hat{B}_\theta \tag{7.65}$$

$$\frac{d\hat{B}_\theta}{dz} = -\frac{j\omega}{c^2} \hat{E}_r - \mu_0 \hat{v}_r \tag{7.66}$$

$$0 = -\gamma \hat{B}_\theta + \frac{j\omega}{c^2} \hat{E}_z + \mu_0(v_0\hat{\rho} + \rho_0 \hat{v}_z) \tag{7.67}$$

$$\frac{d\hat{E}_z}{dz} = \frac{\hat{\rho}}{\epsilon_0} - \gamma \hat{E}_r \tag{7.68}$$

$$\left(j\omega + v_0 \frac{d}{dz}\right)(p\hat{v}_r) = \eta(\hat{E}_r - v_0 \hat{B}_\theta) + \eta B_{0z} \hat{v}_\theta \tag{7.69}$$

$$\left(j\omega + v_0 \frac{d}{dz}\right)(p\hat{v}_z) + \hat{v}_z \frac{d}{dz}(qv_0) = \eta \hat{E}_z \tag{7.70}$$

$$\frac{d\hat{E}_\theta}{dz} = j\omega \hat{B}_r \tag{7.71}$$

$$\frac{d\hat{B}_r}{dz} = -\gamma \hat{B}_z + \frac{j\omega}{c^2} \hat{E}_\theta + \mu_0 \rho_0 \hat{v}_0 \tag{7.72}$$

$$0 = \gamma \hat{E}_\theta + j\omega \hat{B}_z \tag{7.73}$$

$$\left(j\omega + v_0 \frac{d}{dz}\right)(p\hat{v}_\theta) = \eta(\hat{E}_\theta + v_0 \hat{B}_r) - \eta B_{0z} \hat{v}_r \quad . \tag{7.74}$$

We notice that the systems (7.65) - (7.70) and (7.71) - (7.74) become independent when $B_{0z} = 0$. In the case the beam is ion-neutralized, (ρ_0) and (v_0) are constant and $p = (1 - v_0^2/c^2)^{\frac{1}{2}}$, $q = 0$. Assuming all quantities in (7.65) - (7.74) to vary as $e^{-j\beta z}$ and putting $\omega_c = \eta B_{0z}/p$, $\omega_p^2 = \eta\rho_0/(p\epsilon_0)$, $\omega_b = \omega - v_0\beta$, $\epsilon = 1 - (\omega_p/p\omega_b)^2$, the beam determinantal equation becomes:

$$\left(\gamma^2 + \beta^2 - \frac{\omega^2}{c^2} + \frac{\omega_p^2}{c^2}\right)^2 = \frac{\omega_c^2}{\epsilon\omega_b^2}\left(\gamma^2 + \beta^2 - \frac{\omega^2}{c^2}\right)\left[\gamma^2 + \epsilon\left(\beta^2 - \frac{\omega^2}{c^2}\right)\right] . \quad (7.75)$$

Furthermore, in view of (7.64), the free-space equations (7.43), (7.44), and the boundary conditions (7.63) we have:

$$\beta^2 = \frac{\omega^2}{c^2} - \gamma^{+2} \quad (7.76)$$

$$\left[\epsilon\frac{\gamma^+}{\gamma}\frac{J_m'(\gamma b)}{J_m(\gamma b)} - \frac{N_m'(\gamma^+ b)}{N_m(\gamma^+ b)}\right]\left[\frac{\gamma^+}{\gamma}\frac{J_m'(\gamma l)}{J_m(\gamma b)} - \frac{N_m'(\gamma^+ b)}{N_m(\gamma^+ b)}\right]$$

$$= \frac{m^2}{(\gamma b)^2}\left(\epsilon\frac{\gamma^+}{\gamma} - \frac{\gamma}{\gamma^+}\right)\left(\frac{\gamma^+}{\gamma} - \frac{\gamma}{\gamma^+}\right) , \quad (7.77)$$

where (γ^+) refers to the value of (γ) in free-space.

In solving (7.75), (7.76) and (7.77) two approximations will be made. Firstly, we let in the quasi-static approximation that the speed of light (c) approaches infinity. We have verified that the resulting equations.

$$\gamma^2 + \beta^2 = \frac{\omega_c^2}{\epsilon\omega_b^2}(\gamma^2 + \epsilon\beta^2) \quad (7.78)$$

$$\gamma^{+2} + \beta^2 = 0 \quad (7.79)$$

are also obtained when $\nabla \times \hat{E} = 0$ and the terms $(v_0 \hat{B}_\theta)$ and $(\hat{E}_\theta + v_0 \hat{B}_r)$ in (7.69) and (7.74) are neglected. On introducing further the thin-beam approximations

$$J_m'(\gamma b)/J_m(\gamma b) \approx m/(\gamma b)$$
$$N_m'(\gamma^+ b)/N_m(\gamma^+ b) \approx -m/(\gamma^+ b)$$

in (7.77) it is found that, provided $m \neq 0$,

$$\epsilon \approx -1 \tag{7.80}$$

Now from (7.78) (7.79) and (7.80) we have

$$\beta = \frac{1}{v_0}\left(\omega \pm \frac{\omega_p}{\sqrt{2}}\right) \tag{7.81}$$

$$-\beta^2 - \gamma^{+2} = \gamma^2 \frac{1 + 2\frac{\omega_c^2}{\omega_p^2}}{1 - 2\frac{\omega_c^2}{\omega_p^2}} \quad . \tag{7.82}$$

We see that since (ω) is real, (β) is real and hence (γ^+) is imaginary. Further, (γ) is real when $\omega_c^2 < \frac{1}{2}\omega_p^2$ and imaginary when $\omega_c^2 > \frac{1}{2}\omega_p^2$. The case $m = 0$ has already been discussed by Hahn and will therefore not be considered here.

For the space-charge limited case we will at present only consider the quasi-static WKB solutions of Eqs. (7.65) - (7.74). It is convenient to introduce the scalar potential (ϕ) defined by $\vec{E} = -\nabla\phi$, which amounts to putting

$$\hat{E}_r = \gamma\hat{\phi} \ , \ \hat{E}_\theta \approx 0 \ ; \ \hat{E}_z = -\frac{d\hat{\phi}}{dz} \ , \tag{7.83}$$

and furthermore

$$\hat{v}_+ = \hat{v}_r + j\hat{v}_\theta \; ; \; \hat{v}_- = \hat{v}_r - j\hat{v}_\theta \quad . \tag{7.84}$$

The sixth-order system to be solved is then

$$\left(j\omega + v_0 \frac{d}{dz}\right)(\hat{\rho}/\rho_0) = - v_0 \frac{d}{dz}(\hat{v}_z/v_0) - \tfrac{1}{2}\gamma(\hat{v}_+ + \hat{v}_-) \tag{7.85}$$

$$\left(\frac{d^2}{dz^2} - \gamma^2\right)\hat{\phi} = - \hat{\rho}/\epsilon_0 \tag{7.86}$$

$$\left[j(\omega + \omega_c) + v_0 \frac{d}{dz}\right]\hat{v}_+ = \eta\gamma\hat{\phi} \tag{7.87}$$

$$\left[j(\omega - \omega_c) + v_0 \frac{d}{dz}\right]\hat{v}_- = \eta\gamma\hat{\phi} \tag{7.88}$$

$$\left(j\omega + v_0 \frac{d}{dz}\right)(v_0\hat{v}_z) = - \eta v_0 \frac{d\hat{\phi}}{dz} \quad , \tag{7.89}$$

and the first order WKB solution is given by

$$\hat{\phi}(z) = \text{const.} \left[-\beta + \beta \frac{\omega\omega_p^2}{\omega_b^3} + \gamma^2 v_0 \frac{\omega_b}{(\omega_b^2 - \omega_c^2)^2}\frac{\omega_p^2}{\omega_b^2}\right]^{-\frac{1}{2}} e^{-j\int \beta(z)\, dz} \tag{7.90}$$

$$\gamma^2 + \beta^2 = \frac{\omega_c^2}{\epsilon\, \omega_b^2}(\gamma^2 + \epsilon\, \beta^2) \quad . \tag{7.91}$$

Except for $(\omega\ ,\ \omega_c\ ,\ \gamma)$, all quantities are a function of (z) . The ranges of validity and the usefulness of this solution are still being investigated.

Because of limited space we will presently omit further discussion on other methods of solution.

III ELECTRON BEAM INTERACTION WITH A CESIUM PLASMA

A INTRODUCTION

The objectives of this project are to carry out a detailed theoretical and experimental study of the interaction between an electron stream and a plasma. The study includes methods of exciting the interaction. Diagnostic techniques necessary for the experimental work are also being studied.

The experimental work utilizes a plasma produced by the thermal ionization of cesium. The cesium plasma is of relatively low temperature (2300°K), has a high percentage of ionization, is free of many of the oscillations present in discharge plasmas, and allows a well-formed electron beam to pass through it without hitting neutral atoms.

B PRESENT STATUS

In the previous Annual Report, the propagation theory we have developed for a plasma column with a radial density variation was discussed, and the experimental work to check our theory and to learn something about the plasma profile was outlined. Using the experimental configuration of Fig. 8.1 with plasma frequencies generally in L-band or S band, we found that it was possible to obtain very detailed data on the phase characteristics of the forward-wave passband. However, the backward-wave passband for the symmetric mode (i.e., no angular variation in the fields) was not to be found. Since much of our beam-plasma interaction theory and some of our diagnostic theory is based on the existence of this backward-wave passband, the experiment was modified several times and much effort was spent in trying to find and measure the backward wave. Some of the simpler modifications were aimed at improving the detection system by increasing sensitivity and reducing noise. The final detection system could readily detect 90 dbm with certainty. Other modifications included changes in the schemes for

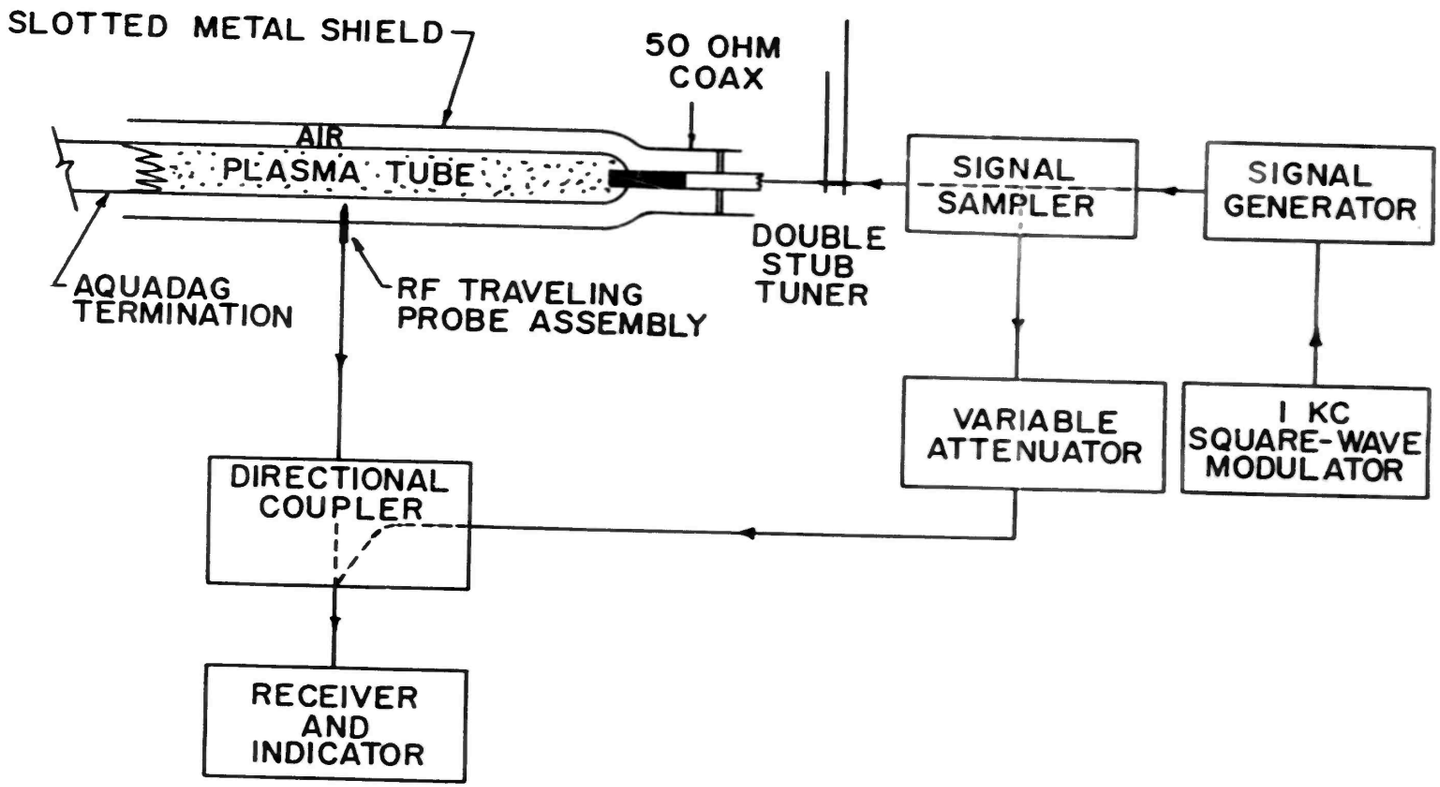

SCHEMATIC DIAGRAM OF EXPERIMENTAL APPARATUS FOR ATTENUATION AND PHASE MEASUREMENTS

FIGURE 8.1.

exciting the wave and/or detecting the wave. In addition, discharge tubes of different radial dimensions were explored, all tubes being made of low-rf-loss glass. The details are discussed at greater length in previous quarterly reports under this contract (Microwave Laboratory Reports Nos. 1012 and 1037). Nevertheless, the backward wave was not conclusively found.

A fast-wave passband was found in the approximate frequency range where the backward-wave passband should have been; these fast waves are not predicted from our slow-wave theory, but it is believed that they propagate along the glass and air space separating the plasma and drift tube. The fast-wave passband is affected by a change in dc magnetic field or a change in plasma density. Therefore, it is unlikely that some "slow" mode, due to the slot in the drift tube, is responsible for the fast-wave passband.

In addition to the fast-wave passband, it was possible to excite a rather weak θ-varying slow-wave mode in the frequency range where the backward-wave passband should have been. This mode is predicted from the theory. It is suspected that earlier workers may have interpreted this θ-varying mode to be the non-θ-varying backward-wave mode. At present, experimental evidence for the existence of the backward wave is scarce and dubious. Some of the evidence is discussed in our previous quarterly reports.

From the detailed phase measurements of the forward-wave passband, both with and without the dc magnetic field, we have sought to determine the cross-sectional profile of the plasma column. Without a dc magnetic field, we find that the propagation characteristics can be quite accurately predicted by assuming the plasma column has a parabolic variation in density

$$n = n_0 \left(1 - \alpha \frac{r^2}{a^2} \right) \tag{8.1}$$

with $\alpha \approx 0.6$. This model and this value of α is in reasonable agreement with a theory by Parker[1] which predicts the radial density

---

[1] J. V. Parker, Electron Tube and Microwave Laboratory Technical Report No. 19, Calif. Inst. of Tech. (December 1963).

distribution of a discharge column. From Fig. 8.2, it may be seen how α appears to be bracketed between 0.5 and 0.6. Analysis of several sets of data appears to indicate a value of $\alpha = 0.57$ would be quite good, but one should not attach too much importance to the second significant figure since the parabolic density distribution is only an approximation to the actual density profile.

When there is no dc magnetic field, the slope near cutoff of the $\omega - \beta$ curve (i.e., the phase velocity at low frequency) is proportional to the average plasma density, the constant of proportionality depending upon the geometry of the system. For the configuration shown in Fig. 8.2, the slope is given by

$$\left(\frac{f}{\beta a}\right)_{f\to 0} = \left[\frac{\ln\frac{b}{a} + \frac{\kappa_2}{\kappa_3}\ln\frac{c}{b}}{2\kappa_2}\right]\overline{\omega_p} \quad , \tag{8.2}$$

where

$$\overline{\omega_p} = \omega_{p0}\sqrt{1 - \frac{\alpha}{2}} \quad . \tag{8.3}$$

Once the value of α was established experimentally to be approximately 0.6, a simple measurement of plasma wavelength for a few values of $\omega \ll \omega_p$ (i.e., near cutoff) was found to be a very convenient diagnostic tool for certain types of experiments.

Trivelpiece[1] assumed, without proof, that the low-frequency phase velocity of waves which propagate in the presence of an axial dc magnetic field also depended only on the average charge density. We have shown that this assumption is in general false, and have derived the correct relation which defines the phase velocity near cutoff. The phase velocity

---

[1] A. W. Trivelpiece, "Slow Wave Propagation in Plasma Waveguides," Electron Tube and Microwave Laboratory Technical Report No. 7, Calif. Inst. of Tech. (May 1958).

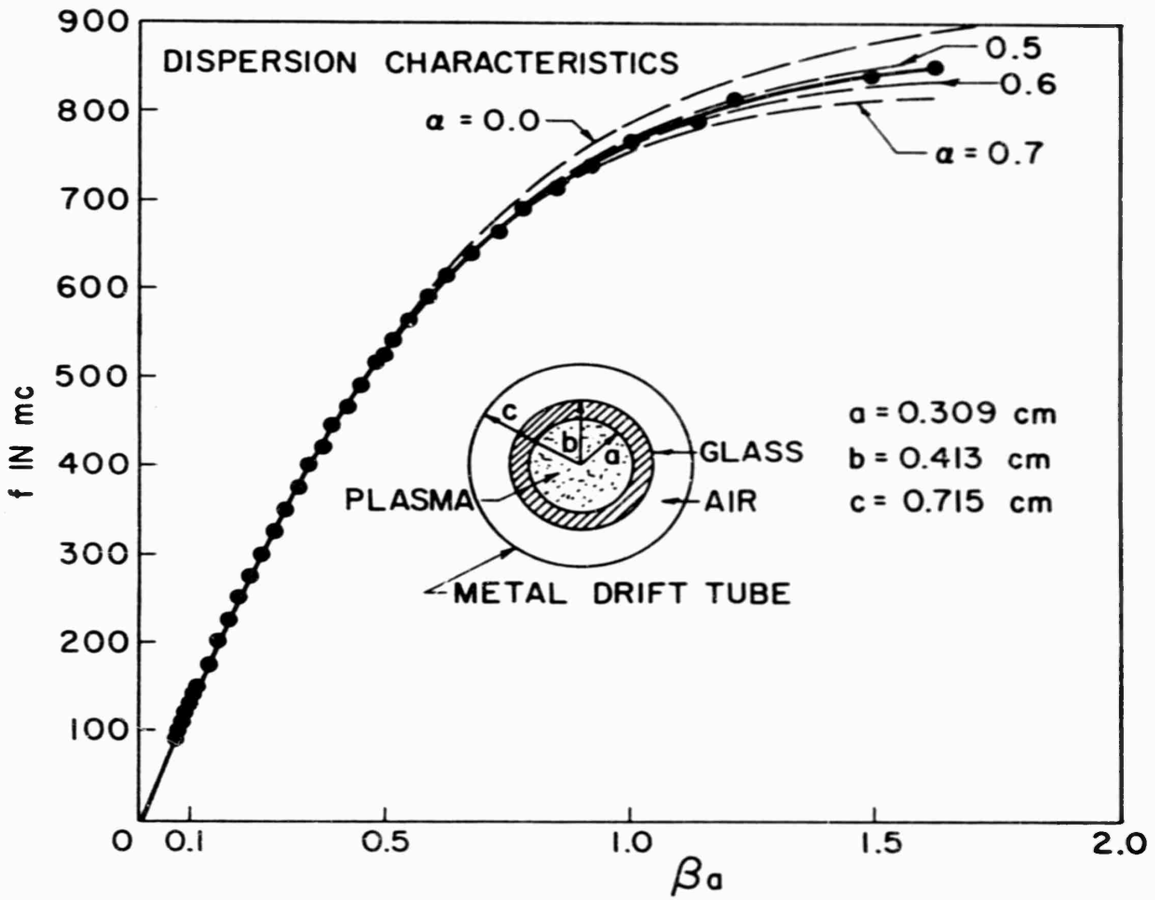
DISPERSION CHARACTERISTICS
α = 0.0
0.5
0.6
α = 0.7
f IN mc
900
800
700
600
500
400
300
200
100
0
0.1
0.5
1.0
1.5
2.0
βa
c
b
a
GLASS
AIR
PLASMA
METAL DRIFT TUBE
a = 0.309 cm
b = 0.413 cm
c = 0.715 cm

FIGURE 8.2.

near cutoff does in general depend on the dc magnetic field. A report is being written covering our entire propagation theory and propagation experiments.

The previous Annual Report discussed some experimental cesium plasma amplifier tubes we had built and an exploratory coupling experiment we had performed. We have now designed two new cesium plasma tubes as part of a program to measure the saturation gain, rf current, and efficiency of a beam-plasma interaction device, and to perform a sophisticated coupling experiment. The two tubes are essentially identical except that one tube has an output cavity designed to couple directly to the beam, whereas the other tube has an output cavity designed to couple to the beam via the plasma (see Fig. 8.3). Both tubes fit into the same experimental apparatus. It is expected that the results from the study of the first tube will serve to eliminate some of the unknowns from the study of the second tube.

Cesium is a corrosive metal and attacks most of the common glass-to-metal disk seals. For that reason, plus the requirement that all metal parts in the tube be nonmagnetic, the cavity disks are made of molybdenum. The glass in the seal is high-temperature alumina silicate. Each tube requires four glass-to-metal seals, two for each cavity disk; therefore, a certain amount of developmental work was required in order to obtain satisfactory seals. We are now able to make the seals quite routinely.

The original tube design has been changed somewhat. Originally a commercial large glass stem with large metal pins was utilized for mounting the plasma heater spirals and back-up plates. The stem cracked several times, both during tube manufacture and during tube operation, because the glass was so thick it could develop large thermal stresses. The tube shown in Fig. 8.3 is the present design. A tube of this design has now been built and a cradle is being made to help support the fragile helix stem.

The theoretical study of the gain mechanism of the finite beam-plasma interaction has progressed. The finite beam and plasma model is shown in Fig. 8.4. The plasma and beam are assumed to be uniform and infinitely long or properly terminated. The dc magnetic field is uniform but of arbitrary magnitude. We have invoked the slow-wave approximation and have

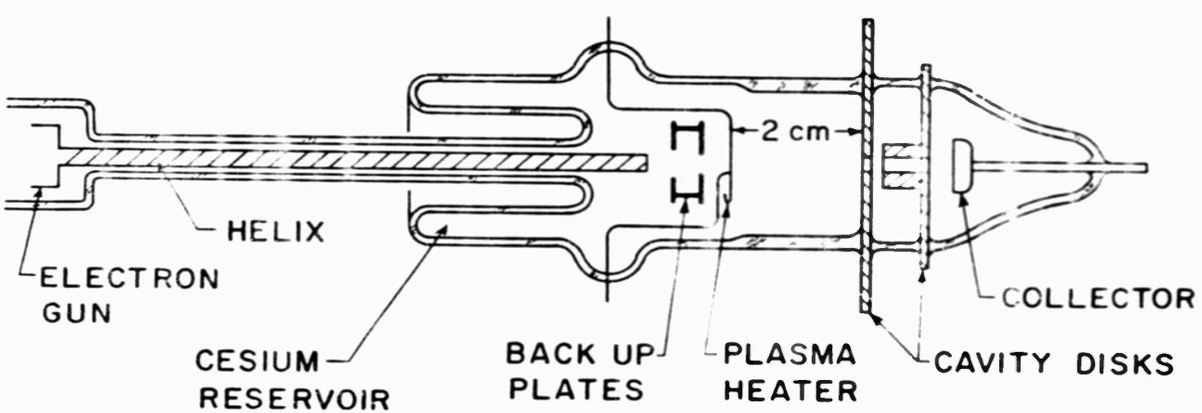

FIG. 8.3--Cross-section of experimental cesium beam-plasma amplifier.

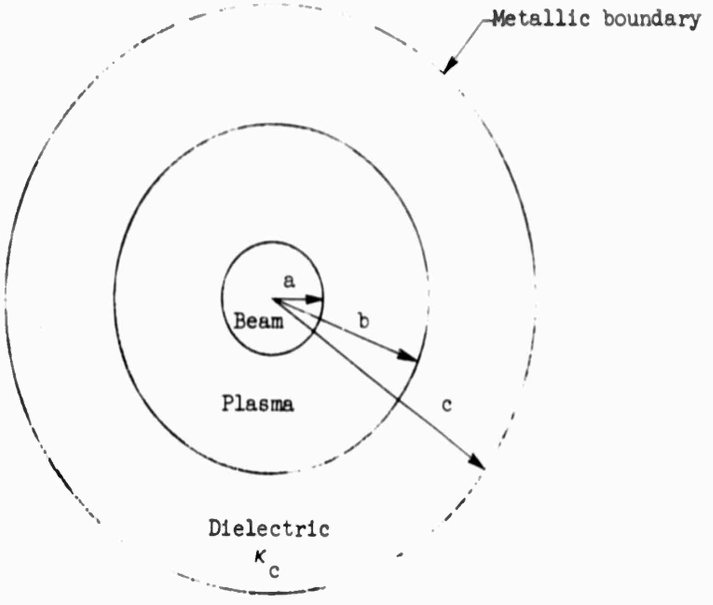

FIG. 8.4--The theoretical model for a general beam-plasma system.

neglected interactions with the cyclotron waves; we feel these approximations are justifiable for the ranges of values we allow our parameters to take. We have considered principally the non-θ-varying modes. Collisions and thermal effects in the plasma and beam are neglected, the maximum gain not being limited by those effects but rather by the finite geometry of the system. Within the framework of our model and our assumptions, several general conclusions may be drawn. We feel that most of these conclusions are quite basic physically and are valid for any beam-plasma model in a dc magnetic field.

The conclusions may be categorized according to the tensor components of the anisotropic dielectric constant of the plasma. They are:

1. In a frequency range where ϵ_{zzp} and ϵ_{rrp} are both positive, there will be no gain (gain due to interactions with the cyclotron waves not being considered).

2. In a frequency range where ϵ_{zzp} and ϵ_{rrp} are both negative, there will be gain of the easitron type (i.e., the inductive wall amplifier type gain).

3. The synchronous waves on the electron beam can interact with propagating plasmaguide modes, including the higher-order radial modes, and result in gain of the traveling-wave tube type or of the backward-wave amplifier type. If synchronism occurs in a frequency range where ϵ_{zzp} is positive, the gain is of the backward-wave amplifier type. If synchronism occurs in a frequency range when ϵ_{zzp} is negative, the gain is of the forward traveling-wave tube type. It is possible to have both easitron type gain and traveling-wave type gain simultaneously for certain system geometries.

These three conclusions, all derived analytically, are borne out by the numerical computer calculations. Utilizing the three basic conclusions, it is then possible to simplify somewhat a qualitative investigation of how other effects not included in the theoretical treatment will affect the gain behavior. For example, the way a longitudinal or radial plasma density variation, or the plasma sheath (now that there is a reasonable rf sheath theory[1]), will affect the gain may be predicted qualitatively, and

---

[1] J. M. Pavkovich and G. S. Kino, "RF Behavior of the Plasma Sheath," Microwave Laboratory Report No. 1077, Stanford University (August 1963).

frequently almost quantitatively. A full report on the gain theory is being written.

The experiments and the theory of the plasma sheath effects on the plasmaguide modes have been completed. A condensed paper was presented at the Fifth Annual Meeting of the American Physical Society, November 1963, and was also prepared as Microwave Laboratory Report No. 1105. The title and abstract follow: "Landau Damping in the Plasma Sheath," by H. L. Stover and G. S. Kino:

"In this paper, a number of measurements of the dispersion characteristics and attenuation of slow waves propagating along a finite plasma column are described. These waves are of the type first described by Trivelpiece. As have earlier workers, we have found that the loss is considerably higher at high frequencies than would be expected due to collisions of electrons with neutrals or ions. In the past, the explanation that has been given for this effect is that electrons collide with the walls of the discharge.

"The work of Pavkovich and Kino, described in an accompanying paper, postulates that there is loss in the sheath due to Landau damping. In that paper, the rf properties of the sheath have been characterized by an impedance, the real part of which can cause attenuation of waves propagating along a plasma column.

"We have carried out a detailed propagation theory which takes account of the radial variation of density in a mercury vapor discharge plasma, and have calculated the attenuation due to the sheath impedance and due to elastic collisions with neutrals. The experimental results are compared with the theory, and appear to be well explained by the hypothesis of Landau damping in the sheath."